

# Quantum Filtering and Analysis of Multiplicities in Eigenvalue Spectra

Zhiyan Ding,<sup>1</sup> Lin Lin,<sup>2,3</sup> Yilun Yang,<sup>2</sup> and Ruizhe Zhang<sup>4</sup>

<sup>1</sup>*Department of Mathematics, University of Michigan, Ann Arbor, Michigan 48109, USA*

<sup>2</sup>*Department of Mathematics, University of California, Berkeley, California 94720, USA*

<sup>3</sup>*Applied Mathematics and Computational Research Division,*

*Lawrence Berkeley National Laboratory, California 94720, USA*

<sup>4</sup>*Department of Computer Science, Purdue University, West Lafayette, Indiana 47907, USA*

(Dated: October 10, 2025)

Fine-grained spectral properties of quantum Hamiltonians, including both eigenvalues and their multiplicities, provide useful information for characterizing many-body quantum systems as well as for understanding phenomena such as topological order. Extracting such information with small additive error is  $\#BQP$ -complete in the worst case. In this work, we introduce QFAMES (Quantum Filtering and Analysis of Multiplicities in Eigenvalue Spectra), a quantum algorithm that efficiently identifies clusters of closely spaced dominant eigenvalues and determines their multiplicities under physically motivated assumptions, which allows us to bypass worst-case complexity barriers. QFAMES also enables the estimation of observable expectation values within targeted energy clusters, providing a powerful tool for studying quantum phase transitions and other physical properties. We validate the effectiveness of QFAMES through numerical demonstrations, including its applications to characterizing quantum phases in the transverse-field Ising model and estimating the ground-state degeneracy of a topologically ordered phase in the two-dimensional toric code model. Our approach offers rigorous theoretical guarantees and significant advantages over existing subspace-based quantum spectral analysis methods, particularly in terms of the sample complexity and the ability to resolve degeneracies.

## I. INTRODUCTION

Understanding the energy spectrum of a Hamiltonian is a central problem in quantum computing, quantum complexity theory, quantum chemistry, and many-body physics. While estimating the ground state energy or a few low-lying excitations is a common task, many physical properties require more fine-grained spectral information. For instance, the ground-state degeneracy (GSD) can indicate the presence of topological order—a hallmark of certain condensed matter phases [1] and a key feature for topological quantum computation [2]. More generally, we are interested in estimating both locations and the multiplicities of eigenvalues.

Despite their fundamental physical relevance, extracting such spectral information is computationally challenging: the Hilbert space dimension grows exponentially with system size, making exact diagonalization infeasible even for modestly sized systems. Indeed, the GSD or eigenstate degeneracy problem is shown to be in the worst case  $\#BQP$ -complete—the counting version of QMA [3]<sup>1</sup>. As a result, we can only hope to solve this problem by leveraging additional assumptions for physically motivated Hamiltonians.

In this work, we tackle this problem by proposing a new quantum algorithm, dubbed Quantum Filtering and Analysis of Multiplicities in Eigenvalue Spectra (QFAMES). Our approach prepares a collection of initial states and leverages their correlated information to estimate the *density of dominant eigenstates* (DODS) defined as

$$\mu_D(E) \propto \sum_{i \in \mathcal{D}} \delta(E - \lambda_i), \quad (1)$$

where  $\{\lambda_i\}_{i \in \mathcal{D}}$  denotes the multiset of dominant energy eigenvalues (counting multiplicity), whose corresponding eigenvectors have sufficiently large overlaps with the subspace spanned by the initial states.

To our knowledge, QFAMES is the first quantum algorithm that can provably estimate the DODS with rigorous theoretical guarantees. Specifically, QFAMES identifies clusters of closely spaced dominant eigenvalues and determines exactly the number of (possibly degenerate) eigenstates within each cluster. The algorithm requires only a single ancilla qubit and employs circuits of short depth, which makes it particularly suitable for the early fault-tolerant regime (see [Theorem IV.1](#)). Furthermore, recent advances [6–10] suggest that even this single ancilla qubit may be eliminated under additional assumptions (see [Section VI](#)).

<sup>1</sup> Ref. [3] showed that exactly computing the density of states (dos) for a local Hamiltonian is  $\#BQP$ -complete, under the promise that no eigenvalue lies near the boundary of the target interval  $[a, b]$ . On the other hand, if one only requires a small multiplicative approximation error but allows an exponentially large additive error, the problem becomes significantly easier. For instance, Refs. [4, 5] apply QPE to the maximally mixed state to sample the spectrum, yielding an efficient estimator for the GSD or dos when the target eigenspace degeneracy is exponentially large. In contrast, we focus on the regime where the target degeneracy is  $\mathcal{O}(1)$ .

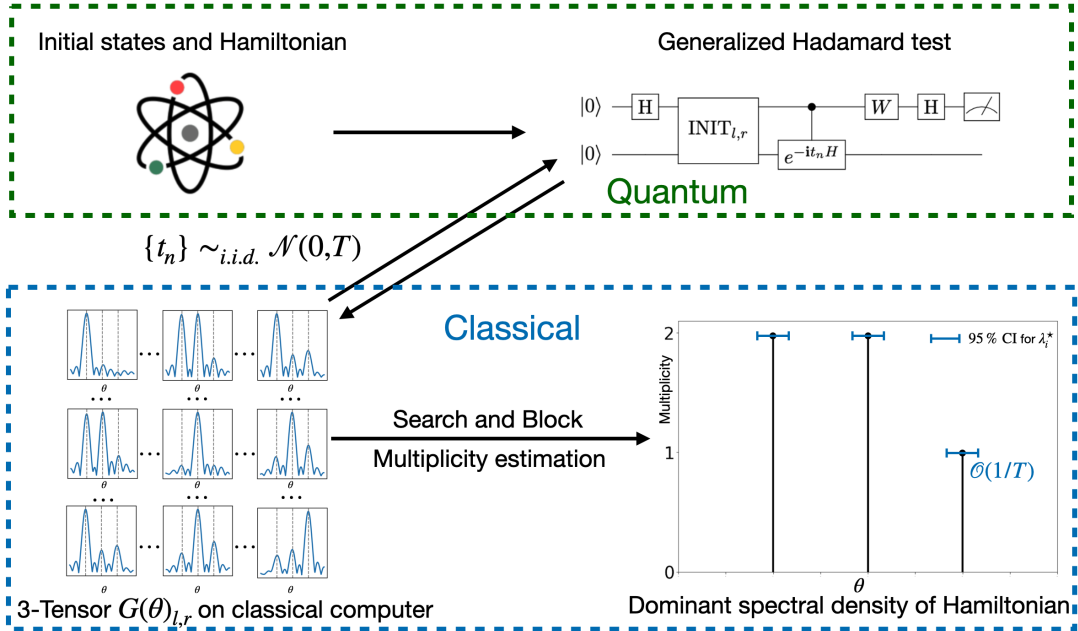


Figure 1: Illustration of the QFAMES algorithm. Given the Hamiltonian and two sets of initial states prepared by circuits  $\{U_l\}_{l \in [L]}$  and  $\{V_r\}_{r \in [R]}$ , we measure quantities of the form  $\mathcal{Z}_{l,r}(t_n) = \langle 0 | U_l^\dagger e^{-iHt_n} V_r | 0 \rangle$  using the generalized Hadamard test circuit. The collected quantum data are then processed classically to (1) estimate the locations of energy eigenstate clusters through searching and blocking, and (2) compute the multiplicities of the probed clusters.

We then extend the algorithm to efficiently estimate expectation values of observables with respect to the dominant eigenstates within a specified cluster. This task may be viewed as a natural generalization of the *eigenstate property estimation* problem [11–14] which focuses solely on a single, isolated eigenstate. Our approach enables probing physical properties within the targeted clusters, thereby providing a useful tool for characterizing phenomena such as quantum phase transitions.

The paper is structured as follows. In Section II, we review the related works. In Section III, we introduce the problem setup and summarize the main results. Section IV presents the QFAMES algorithm in detail, while Section V discusses how to extend the method to extract information of physical observables. Section VI discusses how to implement the QFAMES algorithm in a control-free, ancilla-free setting. In Section VII, we present numerical simulation results with an illustrative example, the transverse field Ising model, and the toric code model. Finally, Section VIII concludes with a discussion of possible future directions.

## II. RELATED WORK

The estimation of Hamiltonian eigenvalues is a fundamental problem in the literature of quantum computation, which can be addressed by a variety of methods collectively known as quantum phase estimation (QPE) algorithms [15–29]. These methods primarily aim at determining the locations of eigenvalues but are inherently incapable of identifying their multiplicities, as they typically assume access to only a single initial state. A more detailed review of these algorithms is provided in Section A.

As will be shown later, our observable eigenstate property estimation problem reduces to a generalized eigenvalue problem, which shares structural similarities with subspace-based quantum eigenvalue estimation methods [30–37]. These subspace methods can be generalized to estimate eigenvalue multiplicities when multiple initial states are used. However, these approaches typically face numerical instabilities when inverting ill-conditioned overlap matrices, and can require high sample complexity to suppress the noise. Compared to the state-of-the-art analysis of subspace methods [34–36], QFAMES avoids the inversion of ill-conditioned matrices by focusing on the dominant eigen-subspaces, and provides much stronger theoretical guarantees for the robustness and the sample complexity of locating the energy eigenvalues. It is also the first work that can provably estimate the eigenvalue multiplicities.

### III. SETUP AND MAIN RESULTS

Let us first formally state the DODS estimation problem:

**Problem III.1** (Density of dominant eigenstates (DODS) estimation). *Let  $H$  be a Hamiltonian with eigen-decomposition  $\{(\lambda_i, |E_i\rangle)\}$ , where, after appropriate normalization, the spectrum satisfies  $\lambda_i \in [-\pi, \pi]$  for all  $i$ . Assume black-box access to controlled time evolution  $e^{-iHt}$  for any  $t \in \mathbb{R}$ , as well as two families of (controlled) state-preparation unitaries  $\{U_\ell\}_{\ell \in [L]}$  and  $\{V_r\}_{r \in [R]}$  satisfying  $U_\ell|0\rangle = |\phi_\ell\rangle$  and  $V_r|0\rangle = |\psi_r\rangle$ .*

We define two overlap matrices  $\Phi \in \mathbb{C}^{L \times M}$  and  $\Psi \in \mathbb{C}^{R \times M}$ :

$$\begin{aligned}\Phi_{l,m} &:= \langle \phi_l | E_m \rangle \quad \forall l \in [L], m \in [M], \\ \Psi_{r,m} &:= \langle \psi_r | E_m \rangle \quad \forall r \in [R], m \in [M].\end{aligned}\tag{2}$$

For each eigenstate  $|E_m\rangle$ , define its overlap with the initial states as:

$$p_m := \|\Phi_{:,m}\|_2 \cdot \|\Psi_{:,m}\|_2.\tag{3}$$

The multiset of dominant eigenvalues, indexed by  $\mathcal{D}$ , consists of those eigenvalues that satisfy the sufficient dominance condition:

$$\left( p_{\min} := \min_{m \in \mathcal{D}} p_m \right) \geq C_p \left( p_{\text{tail}} := \sum_{m \notin \mathcal{D}} p_m \right),\tag{4}$$

for some constant  $C_p$  greater than 1. The distinct dominant eigenvalues are denoted by  $\{\lambda_i^*\}_{i \in [I]}$ , each separated by at least  $\Delta$ , with corresponding eigenvectors indexed by  $\mathcal{D}_i$ . The degeneracies  $|\mathcal{D}_i|$  satisfy  $|\mathcal{D}| = \sum_{i \in [I]} |\mathcal{D}_i|$ .

**Goal:** With high probability, for each  $i \in [I]$ , estimate the dominant eigenvalue  $\lambda_i^*$  within  $\epsilon$ -accuracy and exactly determine its dominant degeneracy  $m_i$ . These outputs together suffice to approximate the density of dominant eigenstates (DODS)  $\mu_D$ , as defined in [Eq. \(1\)](#).

The left and right initial states can be either the same or different, depending on the problem setup. When they are different, the left initial states can be viewed as bases for projective measurements.

If  $\lambda_i$  is a non-degenerate dominant eigenvalue, and there is only one pair of initial states  $|\phi\rangle$  and  $|\psi\rangle$ , then both  $|\langle \phi | E_m \rangle|$  and  $|\langle \psi | E_m \rangle|$  need to be large enough. Indeed, when  $|\phi\rangle = |\psi\rangle$ ,  $p_m = |\langle \phi | E_m \rangle|^2$  is simply the squared overlap between the initial state and the eigenstate, which is the standard assumption in quantum phase estimation and its variants (see [Section A](#)). More generally, if  $\lambda_i$  is a non-degenerate dominant eigenvalue but there are multiple pairs of initial states, then both  $\sum_{l \in [L]} |\langle \phi_l | E_m \rangle|^2 = \|\Phi_{:,m}\|_2^2$  and  $\sum_{r \in [R]} |\langle \psi_r | E_m \rangle|^2 = \|\Psi_{:,m}\|_2^2$  need to be sufficiently large, which states that the eigenstate  $|E_m\rangle$  has non-vanishing overlap with at least one initial state in each set. This can be concisely captured by the condition for  $p_m$  in [Eq. \(3\)](#) and [Eq. \(4\)](#).

In order to compute the multiplicity of a degenerate dominant eigenvalue  $\lambda_i^*$ , we need a stronger condition to ensure that *all* normalized eigenvectors corresponding to the degenerate eigenvalue  $\lambda_i^*$  in the eigenspace  $\mathcal{E}_i := \text{span}\{|E_m\rangle\}_{m \in \mathcal{D}_i}$  have non-vanishing overlap with the set of initial states. In other words, both of the following quantities

$$\min_{|E\rangle \in \mathcal{E}_i, \langle E | E \rangle = 1} \sum_{l \in [L]} |\langle \phi_l | E \rangle|^2, \quad \min_{|E\rangle \in \mathcal{E}_i, \langle E | E \rangle = 1} \sum_{r \in [R]} |\langle \psi_r | E \rangle|^2,\tag{5}$$

need to be sufficiently large. This will be formulated more precisely as a *uniform overlap condition* in [Assumption 1](#) of [Section B](#). Indeed, if one of the quantities in [Eq. \(5\)](#) vanishes, we prove that there is an *information-theoretic barrier* for resolving the degeneracy ([Theorem B.1](#)). As a special case, this proves that existing quantum phase estimation algorithms, which typically use only a single initial state, cannot resolve eigenvalue degeneracies.

The uniform overlap condition states that the overlap of all normalized vectors in the eigen-subspace with the initial states should be uniformly bounded from below. However, this does not require the initial states to be well-conditioned. In fact, we do not even require the vectors  $\{|\phi_l\rangle\}$  (or  $\{|\psi_r\rangle\}$ ) to be *linearly independent*. This provides significantly enhanced flexibility in choosing the initial states compared to existing subspace methods, which typically require the initial states to be a well-conditioned set of vectors. That said, the initial states should not be chosen randomly. In practical calculations, the initial states should be chosen carefully and in a physically motivated manner, such as low-energy states prepared by variational quantum algorithms [38–40], quantum imaginary time evolution [41–43], and the non-orthogonal ansatz states used in the Non-Orthogonal Quantum Eigensolver (NOQE) [31, 35] approach.

The main result of this paper is an efficient quantum algorithm to solve the DODS estimation problem with **rigorous theoretical guarantees**.

**Theorem III.2** (Main result, Informal version of [Theorem IV.1](#)). *There exists a quantum algorithm that repeatedly runs the quantum circuit in [Fig. 1](#) to collect data with Hamiltonian evolution times  $t_1, \dots, t_N \in \mathbb{R}$  such that*

- *maximal evolution time:  $T_{\max} := \max\{|t_n|\} = \tilde{\mathcal{O}}(p_{\text{tail}}\epsilon^{-1})$ ;*
- *total evolution time:  $T_{\text{total}} := \sum_n |t_n| = \tilde{\mathcal{O}}(p_{\text{tail}}^{-1}\epsilon^{-1})$ .*

By classically post-processing the data, it guarantees that for each distinct dominant eigenvalue,

- *its location can be estimated to within  $\epsilon$  accuracy; and*
- *its multiplicity can be determined exactly.*

Note that our algorithm can also resolve dominant eigenvalues that are **approximately degenerate**, i.e., when there is a cluster of dominant eigenvalues lying in a narrow energy interval around  $\lambda_i^*$  with width  $\delta \ll \Delta$ . See more discussion in [Section IV B](#).

As an extension of the algorithm, we also propose an efficient method ([Algorithm 2](#)) for estimating degenerate eigenstate properties in [Section V](#). The problem is defined as follows.

**Problem III.3** (Degenerate eigenstate property estimation). *Let  $O$  be an observable. For each dominant eigenvalue  $\lambda_i^*$ , estimate the eigenvalues of the projected observable  $O_{\mathcal{D}_i}$  in the corresponding subspace:*

$$O_{\mathcal{D}_i} := (\langle E_k | O | E_{k'} \rangle)_{k, k' \in \mathcal{D}_i}, \quad \mathcal{D}_i = \{k \in \mathcal{D} : \lambda_k = \lambda_i^*\}. \quad (6)$$

Let us denote the eigenvalues by  $\lambda_k^O$ . We remark that any value within the range  $[\min_k \lambda_k^O, \max_k \lambda_k^O]$  can be realized by some linear combination of the degenerate eigenstates, and it is thus less useful to estimate  $\langle E_m | O | E_m \rangle$  for each individual dominant eigenstate. For example, in the ferromagnetic phase of a spin chain model, there can be two degenerate ground states  $|E_0\rangle = |\uparrow\uparrow \dots \uparrow\rangle$  and  $|E_1\rangle = |\downarrow\downarrow \dots \downarrow\rangle$ . The measured ground states can be however  $(|E_0\rangle + |E_1\rangle)/\sqrt{2}$  and  $(|E_0\rangle - |E_1\rangle)/\sqrt{2}$ , both of which yield zero average magnetization.

For simplicity, we provide the resource estimation in the case of no tail eigenvalues (i.e.,  $p_{\text{tail}} = 0$ ) and  $p_{\min}$  being bounded below by a constant. To achieve  $\epsilon_O$ -accuracy in estimating each eigenvalue of  $O_{\mathcal{D}_i}$ , it suffices to choose

$$T_{\max} = \tilde{\mathcal{O}}(\Delta^{-1}), \quad T_{\text{total}} = \tilde{\mathcal{O}}(\Delta^{-1}\epsilon_O^{-2}). \quad (7)$$

The proposition showing this result is [Theorem V.1](#) in [Section V](#).

## IV. QFAMES ALGORITHM AND COMPLEXITY ANALYSIS

In this section, we describe the QFAMES algorithm in [Section IV A](#), present its pseudo-code, and provide an illustrative example. A detailed complexity analysis follows in [Section IV B](#).

### A. Algorithmic description

Our goal is to estimate the DODS, including the dominant eigenvalues  $\lambda_i^*$  and corresponding multiplicities  $m_i$ . If we assume the eigenvalues are separated by at least  $\Delta$ , then we can define energy filters of the form  $\exp[-(\theta - H)^2 T^2]$  to filter out the energy eigenstates away from the desired dominant eigenvalue, where the filter width is chosen to be  $T \gtrsim 1/\Delta$ . The filter can be implemented with time evolution operators through sampling from its the Fourier transform

$$e^{-(\theta - H)^2 T^2} = \int e^{i(\theta - H)t} a_T(t) dt, \quad (8)$$

where

$$a_T(t) = \frac{1}{2T\sqrt{\pi}} \exp\left(-\frac{t^2}{4T^2}\right) \quad (9)$$

is the probability density function for evolution time  $t$  (more rigorously, we will sample  $t$  from a truncated Gaussian distribution as defined in [Eq. \(16\)](#) to avoid extremely large  $t_n$ ).

For the given sets of left and right initial states  $|\phi_l\rangle$  and  $|\psi_r\rangle$ , we want to compute the matrix  $\mathcal{G}(\theta)$  with matrix elements

$$\mathcal{G}_{l,r}(\theta) = \langle \phi_l | e^{-(\theta-H)^2 T^2} | \psi_r \rangle . \quad (10)$$

At  $\theta = \lambda_i^*$ , we have

$$\begin{aligned} \mathcal{G}(\lambda_i^*) &= \Phi \cdot \text{diag} \left( \left\{ e^{-(\lambda_i^* - \lambda_m)^2 T^2} \right\}_{m \in [M]} \right) \cdot \Psi^\dagger \\ &\approx \Phi_{:, \mathcal{D}_i} \cdot (\Psi_{:, \mathcal{D}_i})^\dagger, \end{aligned} \quad (11)$$

where the matrices  $\Phi$  and  $\Psi$  are defined in [Eq. \(2\)](#), and  $\Phi_{:, \mathcal{D}_i}$  and  $\Psi_{:, \mathcal{D}_i}$  are the corresponding submatrices that contain the columns of dominant eigenstates with eigenvalue  $\lambda_i^*$ .  $\mathcal{D}_i$  denotes the index set of these eigenvalues. Due to the concentration of  $\exp(-x^2 T^2)$  around zero, this expression implies that only those eigenvalues that are close to  $\lambda_i^*$  contribute significantly to the matrix  $\mathcal{G}(\lambda_i^*)$ , and the remaining eigenvalues are filtered out. Under the uniform overlap assumption ([Assumption 1](#)), we can show that the rank of the matrix  $\mathcal{G}(\lambda_i^*)$  equals the degeneracy of dominant eigenstates at  $\lambda_i^*$ . This is the key insight that enables QFAMES to solve the DODS estimation problem. Specifically:

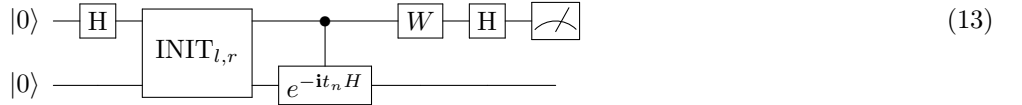
- *Location estimation:* We evaluate the **Frobenius norm** of  $\mathcal{G}(\theta)$  on a uniform grid of  $\theta \in [-\pi, \pi]$ , and use a “searching and blocking” strategy to find the peaks  $\theta_i^*$  of  $\|\mathcal{G}(\theta)\|_F$ . Each peak corresponds to a distinct dominant eigenvalue  $\lambda_i^*$ .
- *Multiplicity estimation:* For each candidate dominant eigenvalue  $\theta_i^*$ , we compute the **numerical rank** of  $\mathcal{G}(\theta_i^*)$  (the number of singular values above some threshold) as the estimated multiplicity.

The detailed description of the algorithm is as follows. The first stage of the algorithm, consisting of Steps 1–3, focuses on estimating the locations of the dominant eigenvalues. The second stage, Step 4, focuses on determining the multiplicity of each dominant eigenvalue.

*Step 1: Generate data.* To obtain Eq. (10), we need to measure quantities of the form

$$\mathcal{Z}_{l,r}(t_n) := \langle 0 | U_l^\dagger e^{-\mathbf{i} H t_n} V_r | 0 \rangle = \langle \phi_l | e^{-\mathbf{i} H t_n} | \psi_r \rangle. \quad (12)$$

They can be obtained with the generalized Hadamard test as drawn below:



Given  $U_l, V_r$ , and  $t_n$ , the measurement outcomes  $Z_{l,r,n}$  of the circuit Eq. (13) provide an unbiased estimator for  $\mathbb{E}[Z_{l,r,n}] = Z_{l,r}(t_n)$ . Using the generalized Hadamard test, we can efficiently gather these measurement outcomes for every pair of  $(U_l, V_r)$  at the Hamiltonian evolution times  $t_1, \dots, t_N$  and formulate them into a 3-order tensor  $Z \in \mathbb{C}^{L \times R \times N}$ :

$$\mathbb{E}[Z_{l,r,n}] = \sum_{m \in [M]} \Phi_{l,m} \cdot e^{-i\lambda_m t_n} \cdot (\Psi_{r,m})^* . \quad (15)$$

where  $\Phi$  and  $\Psi$  are the overlap matrices defined in Eq. (2).

The times  $t_1, \dots, t_N$  are sampled independently from the Gaussian probabilistic density function  $a_T(t)$ . In practice, we may truncate the density function to ensure that the maximal runtime is always bounded by  $\sigma T$ :

$$a_T^{\text{trunc}}(t) = \left( 1 - \int_{-\sigma T}^{\sigma T} \frac{1}{2T\sqrt{\pi}} \exp\left(-\frac{s^2}{4T^2}\right) \mathbf{1}_{[-\sigma T, \sigma T]}(s) ds \right) \delta_0(t) + \frac{1}{2T\sqrt{\pi}} \exp\left(-\frac{t^2}{4T^2}\right) \mathbf{1}_{[-\sigma T, \sigma T]}(t), \quad (16)$$

where  $\sigma$  is an adjustable parameter and  $\delta_0(t)$  is the delta function at point 0. Its Fourier transform approximates a Gaussian function and is concentrated around zero.

*Step 2: Compute the filtered density function.* We can now **contract** the time dimension of the data tensor with the following complex exponential vector:

$$\frac{1}{N} [e^{i\theta t_1} \ e^{i\theta t_2} \ \dots \ e^{i\theta t_N}], \quad (17)$$

for a location parameter  $\theta \in \mathbb{R}$  and chosen time samples  $t_1, \dots, t_N$ . This yields an  $L$ -by- $R$  matrix  $G(\theta)$ , where

$$G(\theta)_{l,r} = \frac{1}{N} \sum_{n=1}^N Z_{l,r,n} e^{i\theta t_n}, \quad l \in [L], r \in [R]. \quad (18)$$

Since  $t_1, \dots, t_N$  are sampled independently from the truncated Gaussian probabilistic density function  $a_T^{\text{trunc}}(t)$ , it holds that

$$\begin{aligned} \mathbb{E}[G(\theta)] = \mathcal{G}(\theta) &= \Phi \cdot \text{diag} \left( \left\{ \int e^{i(\theta - \lambda_m)t} a_T^{\text{trunc}}(t) dt \right\}_{m \in [M]} \right) \cdot \Psi^\dagger \\ &\approx \Phi \cdot \text{diag} \left( \left\{ \exp(-(\theta - \lambda_m)^2 T^2) \right\}_{m \in [M]} \right) \cdot \Psi^\dagger. \end{aligned} \quad (19)$$

*Step 3: Search and block.* After computing  $G(\theta)$ , the dominant eigenvalues are identified as the peaks of  $\|G(\theta)\|_F$  and can be located using the search-and-block procedure proposed in [23]. This strategy consists of two iterative components—the search step and the block step—which are described as follows:

- *Search:* In the first step, we find the maximum point  $\theta_1^*$  of  $\|G(\theta)\|_F$ , which approximates to one of the dominant eigenvalues.
- *Block:* To approximate the next dominant eigenvalue and avoid repetition, we define a block interval

$$\mathcal{I}_{B,1} = [\theta_1^* - \alpha/T, \theta_1^* + \alpha/T] \quad (20)$$

for some given constant  $\alpha$ . The conditions for  $\alpha$  are stated in [Theorem IV.1](#). In the following steps, we will not find any points from this interval.

- *Second iteration:* In the second iteration, we find the second maximal point  $\theta_2^*$  of  $\mathcal{G}(\theta)$  outside the block interval  $\mathcal{I}_{B,1} = [\theta_1^* - \alpha/T, \theta_1^* + \alpha/T]$  around  $\theta_1^*$ :

$$\theta_2^* = \arg \max_{\theta \in \mathcal{I}_{B,1}^c} \|G(\theta)\|_F. \quad (21)$$

After obtaining  $\theta_2^*$ , we enlarge the block interval by setting  $\mathcal{I}_{B,2} = [\theta_2^* - \alpha/T, \theta_2^* + \alpha/T] \cup \mathcal{I}_{B,1}$ , and then identify the third maximum of  $\|G(\theta)\|_F$  outside  $\mathcal{I}_{B,2}$ . This searching and updating process is iteratively repeated until a set of  $\tilde{I}$  “maximal” points is discovered. Ultimately, we obtain an approximate candidate set  $\{\theta_i^*\}_{i=1}^{\tilde{I}}$  corresponding to the set of dominant eigenvalues  $\{\lambda_i^*\}_{i \in [I]}$ .

*Step 4: Estimate multiplicity.* For each  $\{\theta_i^*\}_{i=1}^{\tilde{I}}$ , we perform the singular value decomposition

$$\mathcal{G}(\theta_i^*) = U_i \Sigma_i V_i^\dagger, \quad (22)$$

and define

$$m_i = \# \{j \mid (\Sigma_i)_{j,j} > \tau\} \quad (23)$$

for some given threshold  $\tau$ , which gives the multiplicity associated with each candidate  $\theta_i^*$ . If  $m_i = 0$ , then  $\theta_i^*$  corresponds to a spurious dominant eigenvalue and should be discarded.

*Pseudocode.* [Fig. 2](#) summarizes the QFAMES workflow as a tensor network. The left/right blocks  $U_l$  and  $V_r$  prepare two families of initial states. Time evolution  $e^{-iHt}$  induces cross-correlations between these families, which (via the generalized Hadamard test) yield the sampled signals  $Z_{l,r}(t_n)$ . A time-domain filter  $a_T(t)$  and a discrete Fourier transform produce frequency-domain matrices  $F(\theta)$ , which are then processed classically: a search-and-blocking step estimates the distinct dominant eigenvalues  $\{\lambda_i^*\}$ , and rank/conditioning tests on submatrices determine multiplicities  $\{m_i\}$ . An optional branch forms projected observable matrices and solves a generalized eigenvalue problem to obtain the spectrum of  $O_{D_i}$  for each  $\lambda_i^*$ . The detailed algorithm for eigenvalue and multiplicity estimation is presented in [Algorithm 1](#), while the observable estimation will be discussed in detail in [Section V](#).

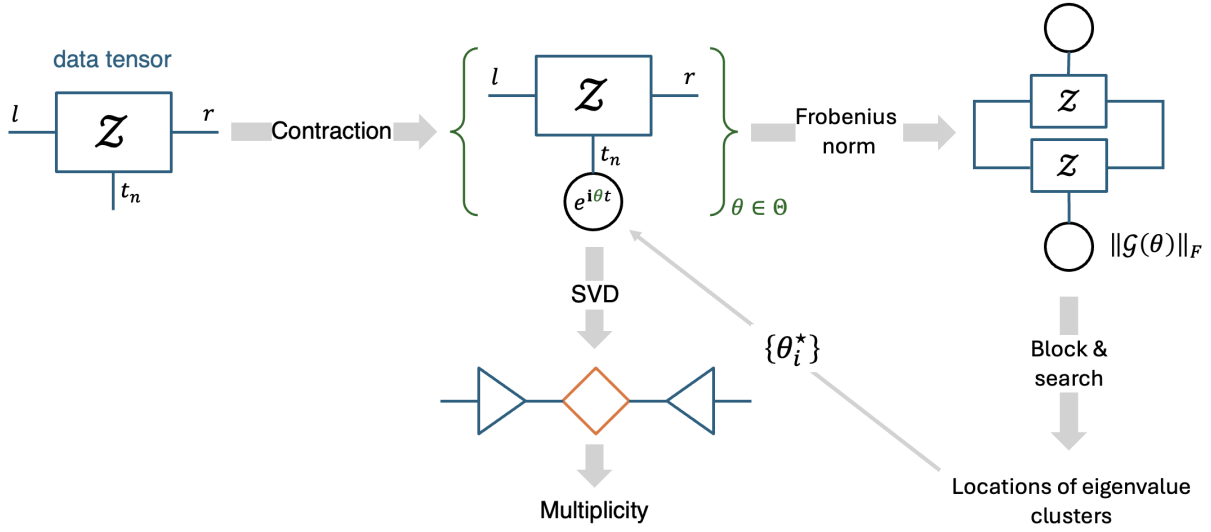


Figure 2: Diagram of the QFAMES algorithm for post-processing the 3-tensor generated from quantum data of the generalized Hadamard test circuit. Left/right tensors  $U_l$  and  $V_r$  prepare initial-state families; the middle leg represents time evolution  $e^{-iHt}$  and data acquisition of cross-correlators  $Z_{l,r}(t_n)$ . A filter  $a_T(t)$  and discrete Fourier transform yield  $\mathcal{G}(\theta)$ , which is post-processed by search-and-blocking to locate dominant eigenvalues  $\{\lambda_i^*\}$  and by rank tests to determine multiplicities  $\{m_i\}$ .

---

**Algorithm 1** Quantum Filtering and Analysis of Multiplicities in Eigenvalue Spectra (QFAMES)

---

1: **Preparation:**  
 Number of data pairs:  $N$ ; Two initial state sets:  $\{\phi_i\}_{i=1}^L$  and  $\{\psi_j\}_{j=1}^R$ ;  
 Filter parameter:  $T$ ; Truncation parameter in Gaussian density  $a_T^{\text{trunc}}$ :  $\sigma$ ;  
 Number of dominant eigenvalues (guess):  $\tilde{I}$ ; Singular value decomposition (SVD) threshold:  $\tau$ .  
 Searching parameter:  $q$  (we search with discrete energy step  $q/T$ );  
 Block parameter:  $\alpha$  (distinct dominant eigenvalues are at least separated by  $\alpha/T$ );

2: **Running:**

3: **Stage I: Estimate the location of dominant eigenvalues**

4: ▷ Step 1: Generate data

5: Sample  $\{t_n\}$  i.i.d. from the truncated Gaussian distribution  $a_T^{\text{trunc}}(t)$  defined in Eq. (16)

6: **for**  $l = 1$  to  $L$  **do**

7:   **for**  $r = 1$  to  $R$  **do**

8:     **for**  $n = 1$  to  $N$  **do**

9:       Generate data  $Z_{l,r,n} \in \{\pm 1 \pm i\}$  using the generalized Hadamard test with  $(U_l, V_r, t_n)$

10:     **end for**

11:   **end for**

12: **end for**

13: ▷ Step 2: Compute the filtered density function

14:  $J \leftarrow \left\lfloor \frac{2\pi T}{q} \right\rfloor$ .

15: Generate discrete candidates:  $\theta_j \leftarrow -\pi + \frac{jq}{T}$  for  $j = 1, 2, \dots, J$ .

16: Calculate

$$\|G(\theta_j)\|_F \leftarrow \left\| \frac{1}{N} \sum_{n=1}^N Z_n \exp(i\theta_j t_n) \right\|_F, \quad 0 \leq j \leq J.$$

17: ▷ Step 3: Search-and-block

18: Block set:  $\mathcal{B}_1 \leftarrow \emptyset$ .

19: **for**  $i = 1$  to  $\tilde{I}$  **do**

20:    $j_i = \text{argmax}_{\theta_j \notin \mathcal{B}_i} \|G(\theta_j)\|_F$ .

21:    $\theta_i^* \leftarrow \theta_{j_i}$ .

---

```

22:  $\mathcal{B}_{i+1} \leftarrow \mathcal{B}_i \cup (\theta_i^* - \frac{\alpha}{T}, \theta_i^* + \frac{\alpha}{T}).$  ▷ Block interval to avoid finding the same peak
23: end for
24: Output: Distinct dominant eigenvalues:  $\{\theta_i^*\}_{i=1}^{\tilde{I}}$ 
25:
26: Stage II: Estimate the multiplicity of each dominant eigenvalue ▷ Step 4: Estimate multiplicity
27:
28: for  $i = 1$  to  $\tilde{I}$  do
29:   Calculate SVD of the data matrix at each  $\theta_i^*:$ 

```

$$U_i \Sigma_i V_i^\dagger = \text{SVD} \left( \frac{1}{N} \sum_{n=1}^N Z_n \exp(\mathbf{i} \theta_i^* t_n) \right)$$


---

```

30:    $m_i = \# \{j \mid (\Sigma_i)_{j,j} > \tau\}.$ 
31: end for
32: Output: Multiplicities:  $\{m_i\}_{i=1}^{\tilde{I}}$ .

```

In the above algorithm,  $\sigma T$  denotes the maximal Hamiltonian simulation time used in the generalized Hadamard test, and  $N$  is the number of repetitions for **each** entry estimation. Therefore, the total Hamiltonian simulation time is upper bounded by  $LR\sigma TN$ . The importance of off-diagonal entries in the data tensor  $Z$  for resolving spectral multiplicities is demonstrated through a concrete illustrative example in [Section VII A](#).

Besides Gaussian functions, we may also use the Kaiser windows and the discrete prolate spheroidal sequence (DPSS/Slepian) windows [44–46] to further suppress spectral leakage and sharpen cluster localization. We leave a detailed study of this to future work.

## B. Complexity analysis

In this section, we analyze the theoretical complexity of the QFAMES algorithm introduced in [Section IV A](#). Recall the overlaps of the dominant eigenvalues and tails defined as [Eq. \(4\)](#):

$$\begin{aligned} p_{\min} &= \min_{m \in \mathcal{D}} \sqrt{\left( \sum_{l=1}^L |\Phi_{l,m}|^2 \right) \left( \sum_{l=1}^R |\Psi_{l,m}|^2 \right)}, \\ p_{\text{tail}} &= \sum_{m \notin \mathcal{D}} \sqrt{\left( \sum_{l=1}^L |\Phi_{l,m}|^2 \right) \left( \sum_{l=1}^R |\Psi_{l,m}|^2 \right)}, \end{aligned} \tag{24}$$

The main theorem on the performance guarantees of the QFAMES algorithm is stated as follows:

**Theorem IV.1.** *Assume the uniform overlap condition ([Assumption 1](#)) hold true,  $p_{\text{tail}}/p_{\min}$  is sufficiently small, and the parameters in [Algorithm 1](#) satisfy the following conditions:*

$$\begin{aligned} N &= \tilde{\Omega}(LRp_{\text{tail}}^{-2}), \quad T = \tilde{\Omega}(1/\Delta), \quad \sigma = \tilde{\Omega}(1), \quad \tilde{I} \geq I, \quad \tau = \Theta(p_{\text{tail}}), \\ q &= \mathcal{O} \left( \frac{p_{\text{tail}}}{(1+\sigma)\sqrt{|\mathcal{D}|LR}} \right), \quad \alpha = \Omega \left( \log \left( \frac{|\mathcal{D}|LR}{p_{\text{tail}}} \right) \right), \quad \alpha = \mathcal{O}(\Delta T). \end{aligned} \tag{25}$$

Given failure probability  $\eta \in (0, 1)$ , up to a permutation of subindices, with probability at least  $1 - \eta$ , we have

$$\lambda_i^* \in [\theta_i^* - \epsilon, \theta_i^* + \epsilon], \quad \forall 1 \leq i \leq I, \tag{26}$$

where the confidence interval length  $\epsilon$  is given by

$$\epsilon = \tilde{\mathcal{O}} \left( \frac{p_{\text{tail}}}{p_{\min}} \cdot \frac{1}{T} \right), \tag{27}$$

and

$$m_i = |\mathcal{D}_i|, \quad 1 \leq i \leq I, \quad m_i = 0, \quad I < i \leq \tilde{I}. \tag{28}$$

We defer a more general and rigorous version of the above theorem, along with its proof, to [Section C](#). The above theorem shows that [Algorithm 1](#) can accurately estimate the locations of the dominant eigenvalues and exactly identify the multiplicity of dominant eigenvalues. Note that the conditions on  $T, N, \sigma, q$ , and  $\alpha$  are similar to those in [23, Theorem 3.2] (see detailed discussion in [Theorem C.3](#)), and the choice of  $\tau$  plays a crucial role in filtering out non-dominant eigenvalues.

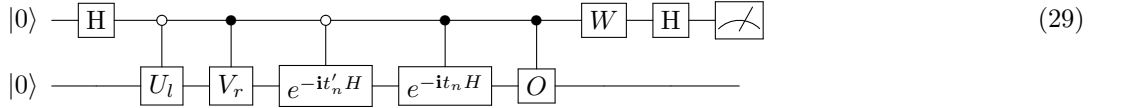
It can be directly obtained from [Theorem IV.1](#) that the maximal evolution time  $T_{\max} = \sigma T = \tilde{\mathcal{O}}(p_{\text{tail}}\epsilon^{-1})$ , and the total evolution time  $T_{\text{total}} = \mathcal{O}(NLRT_{\max}) = \tilde{\mathcal{O}}(L^2R^2p_{\text{tail}}^{-1}\epsilon^{-1})$ . When  $p_{\text{tail}}$  is close to zero, however, the maximal evolution time will instead reach the bound from below as  $T_{\max} = \tilde{\Omega}(\Delta^{-1})$ . In this case, we can use a looser constant  $c = \tilde{\Theta}(\Delta^{-1}\epsilon)$  to replace  $p_{\text{tail}}$  in the scalings and the total evolution time will consequently scale as  $T_{\text{total}} = \tilde{\mathcal{O}}(L^2R^2\Delta\epsilon^{-2})$ . Note that we aim to resolve the gap  $\Delta$  between distinct dominant eigenvalues, which implicitly indicates that  $\Delta > \epsilon$ .

Furthermore, our algorithm also applies to the case of approximately degenerate dominant eigenvalues, where a cluster of such eigenvalues lies within a narrow interval of width  $\delta \ll \Delta$  around  $\lambda_i^*$ . In this setting, the algorithm can efficiently identify the locations of the clusters and determine the exact number of dominant eigenvalues in each. The corresponding assumptions and results are presented in detail in [Section C](#).

## V. EXTENSION TO OBSERVABLE MEASUREMENTS

Within each located dominant eigenvalues, other than multiplicity, more meaningful information can be encoded in expectation values of physical observables. In this section, we will show that it can also be extractable under the QFAMES framework.

The main idea is to slightly modify our circuit to include the observables. Given an observable  $O$ , it can always be rewritten as the weighted sum of unitary Hermitian operators such as Pauli matrices. We can thus assume  $O$  to be unitary without loss of generality. The measurement outcomes  $Z_{l,r,n}^O$  of the modified circuit



provides an unbiased estimator of

$$\mathbb{E}[Z_{l,r,n}^O] = Z_{l,r}^O(t_n, t'_n) := \langle \phi_l | e^{iHt'_n} O e^{-iHt_n} | \psi_r \rangle. \quad (30)$$

Analogous to the QFAMES algorithm, the next step is to contract the two time dimensions of the 3-tensor  $Z_{l,r,n}^O$  with different complex exponential vectors

$$\frac{1}{N} [e^{i\theta t_1} \ e^{i\theta t_2} \ \dots \ e^{i\theta t_N}] \text{ and } \frac{1}{N} [e^{-i\theta t'_1} \ e^{-i\theta t'_2} \ \dots \ e^{-i\theta t'_N}], \quad (31)$$

where both  $\{t_n\}$  and  $\{t'_n\}$  are sampled independently from the truncated Gaussian density distribution  $a_{T/\sqrt{2}}^{\text{trunc}}(t)$  defined in [Eq. \(16\)](#). This results in an  $L$ -by- $R$  matrix

$$G^O(\theta)_{l,r} = \frac{1}{N} \sum_{n=1}^N Z_{l,r,n}^O e^{i\theta t_n} e^{-i\theta t'_n} \quad \forall l \in [L], r \in [R], \quad (32)$$

whose expectation values are

$$\begin{aligned} \mathbb{E}(G^O(\theta)_{l,r}) &= \mathbb{E} \left[ \langle \phi_l | e^{i(H-\theta)t'_n} O e^{-i(H-\theta)t_n} | \psi_r \rangle \right] \\ &= \langle \phi_l | \mathbb{E} \left[ e^{i(H-\theta)t'_n} \right] O \mathbb{E} \left[ e^{-i(H-\theta)t_n} \right] | \psi_r \rangle \\ &= \langle \phi_l | e^{-(\theta-H)^2 T^2/2} O e^{-(\theta-H)^2 T^2/2} | \psi_r \rangle \\ &= \Phi \cdot \text{diag} \left( \left\{ e^{-(\theta-\lambda_k)^2 T^2/2} \right\}_{k \in [M]} \right) \cdot O_{[M]} \cdot \text{diag} \left( \left\{ e^{-(\theta-\lambda_{k'})^2 T^2/2} \right\}_{k' \in [M]} \right) \cdot \Psi^\dagger, \end{aligned} \quad (33)$$

where the matrix  $O_{[M]} := (\langle E_k | O | E_{k'} \rangle)_{k,k' \in [M]}$  is written in the Hamiltonian eigenstate basis. In the second equality, we use the fact that  $t_n, t'_n$  are independent random variables. If we use the truncated Gaussian density distribution, in Eq. (33) the third equal sign should be instead an approximately equal sign.

Let us focus on degenerate dominant eigenstates located at  $\theta_i$  given by [Algorithm 1](#) with multiplicity  $m_i$ . Recall that we have obtained the SVD  $G(\theta_i) = U_i \Sigma_i V_i^\dagger$ , and can thus restrict the matrices  $G(\theta_i)$  and  $G^O(\theta_i)$  to the large singular value subspace with cutoff threshold  $\tau$ :

$$\tilde{G}(\theta_i) = ((U_i)_{:, [m_i]})^\dagger \cdot G(\theta_i) \cdot ((V_i)_{:, [m_i]}) = (\Sigma_i)_{[m_i]} \quad (34)$$

$$\tilde{G}^O(\theta_i) = ((U_i)_{:, [m_i]})^\dagger \cdot G^O(\theta_i) \cdot ((V_i)_{:, [m_i]}), \quad (35)$$

where  $(\Sigma_i)_{[m_i]}$  is the diagonal matrix of  $m_i$  singular values of  $G(\theta_i)$  that are larger than the SVD threshold  $\tau$ , and  $(U_i)_{:, [m_i]}$  and  $(V_i)_{:, [m_i]}$  are the submatrices of  $U_i$  and  $V_i$  that contain the corresponding columns. The rest is to solve the generalized eigenvalue problem

$$\tilde{G}^O(\theta_i)w = \lambda^O \tilde{G}(\theta_i)w \quad (36)$$

with regard to a low dimension, full rank matrix  $G(\theta_i)$ , and the resulting eigenvalues  $\lambda_1^O, \dots, \lambda_{m_i}^O$  will be approximately those of the matrix

$$O_{\mathcal{D}_i} := (\langle E_k | O | E_{k'} \rangle)_{k, k' \in \mathcal{D}_i}, \quad \mathcal{D}_i = \{k \in \mathcal{D} : \lambda_k \in \mathcal{I}_i\}, \quad (37)$$

which is the projection of  $O_{[M]}$  onto the subspace spanned by the dominant eigenstates indexed by  $\mathcal{D}_i$  with eigenvalue  $\lambda_i^*$ . Within the corresponding dominant eigenvector subspace  $\mathcal{E}_i$ , the possible range of expectation values of observable  $O$  can thus be estimated as  $[\min_k \lambda_k^O, \max_k \lambda_k^O]$ .

The correctness of this result can be justified as follows. When  $T$  is large enough and the random noise is negligible, we have

$$G(\theta_i) \approx \Phi_{:, [m_i]} \cdot \text{diag} \left( \left\{ e^{-(\theta_i - \lambda_k)^2 T^2} \right\}_{k \in [m_i]} \right) \cdot (\Psi_{:, [m_i]})^\dagger. \quad (38)$$

Thus, there must exist two invertible matrices  $P_U \in \mathbb{C}^{|m_i| \times |m_i|}$  and  $P_V \in \mathbb{C}^{|m_i| \times |m_i|}$  such that

$$\Phi_{:, [m_i]} = (U_i)_{:, [m_i]} P_U, \quad \Psi_{:, [m_i]} = (V_i)_{:, [m_i]} P_V. \quad (39)$$

Plugging this into the formula of  $\tilde{G}^O(\theta_i)$  and  $\tilde{G}(\theta_i)$ , we obtain

$$\tilde{G}^O(\theta_i) = P_U \cdot \text{diag} \left( \left\{ e^{-(\theta_i - \lambda_k)^2 T^2 / 2} \right\}_{k \in [m_i]} \right) \cdot O_{\mathcal{D}_i} \cdot \text{diag} \left( \left\{ e^{-(\theta_i - \lambda_{k'})^2 T^2 / 2} \right\}_{k' \in [m_i]} \right) \cdot P_V^\dagger, \quad (40)$$

and

$$\tilde{G}(\theta_i) = P_U \cdot \underbrace{\text{diag} \left( \left\{ e^{-(\theta_i - \lambda_k)^2 T^2 / 2} \right\}_{k \in [m_i]} \right)}_{\text{full rank}} \cdot \underbrace{\text{diag} \left( \left\{ e^{-(\theta_i - \lambda_{k'})^2 T^2 / 2} \right\}_{k' \in [m_i]} \right)}_{\text{full rank}} \cdot P_V^\dagger. \quad (41)$$

Compare the above two formulas, it is straightforward to see that the generalized eigenvalue problem in Eq. (36) will give eigenvalues of  $O_{\mathcal{D}_i}$ .

---

**Algorithm 2** Extracting observable expectation values under the QFAMES framework

---

1: **Preparation:**

Number of data pairs:  $N$ ; Two initial state sets:  $\{\phi_i\}_{i=1}^L$  and  $\{\psi_j\}_{j=1}^R$ ;

Filter parameter:  $T$ ; Truncation parameter in Gaussian density  $a_T^{\text{trunc}}$ :  $\sigma$ ;

Unitary observable:  $O$ ;

Output from [Algorithm 1](#):

Location of degenerate dominant eigenvalue:  $\theta_i$ ; Degeneracy:  $m_i$ ;

SVD result of  $G(\theta_i)$ :  $G(\theta_i) = U_i \Sigma_i V_i^\dagger$ .

2: **Running:**

3:

▷ **Step 1: Generate data**

4: Sample  $\{t_n\}$  and  $\{t'_{n'}\}$  i.i.d. from the truncated Gaussian distribution  $a_{T/\sqrt{2}}(t)$  defined as Eq. (16)

```

5: for  $l = 1$  to  $L$  do
6:   for  $r = 1$  to  $R$  do
7:     for  $n = 1$  to  $N$  do
8:       Generate  $Z_{l,r,n} \in \{\pm 1 \pm \mathbf{i}\}$  using generalized Hadamard test with  $(U_l, V_r, t_n, t'_n, O)$ 
9:     end for
10:   end for
11: end for ▷ Step 2: Solve the generalized eigenvalue problem
12:
13: Calculate matrices

```

$$\begin{aligned}\tilde{G}^O(\theta_i) &= ((U_i)_{:, [m_i]})^\dagger \cdot G^O(\theta_i) \cdot ((V_i)_{:, [m_i]}) \\ \tilde{G}(\theta_i) &= ((U_i)_{:, [m_i]})^\dagger \cdot G(\theta_i) \cdot ((V_i)_{:, [m_i]}) = (\Sigma_i)_{[m_i]},\end{aligned}$$

14: Solve the generalized eigenvalue problem

$$\tilde{G}^O(\theta_i)w = \lambda^O \tilde{G}(\theta_i)w.$$

15: **Output:** Eigenvalues:  $\{\lambda_k^O\}_{k=1}^{m_i}$  that provide estimations of eigenvalues of  $O_{\mathcal{D}_i}$ .

Below we will provide an informal resource analysis for the observable estimation algorithm. For simplicity, we focus on the second regime we discussed in the end of [Section IV B](#). The proof is given in [Appendix D](#).

**Proposition V.1.** *In additional to the assumption in [Theorem IV.1](#), assume that  $|\mathcal{D}_i|, L, R = \mathcal{O}(1)$ , access to a Pauli observable  $O$ , and*

1.  $p_{\min} = \Omega(1)$ , which is reflected by the SVD threshold  $\tau$  in the algorithm;
2. there are no tail eigenvalues, i.e.,  $p_{\text{tail}} = 0$ .

To achieve  $\epsilon_O$ -accuracy in estimating eigenvalues of  $O_{\mathcal{D}_i}$ , it suffices to choose

$$T_{\max} = \tilde{\mathcal{O}}(\Delta^{-1}), \quad N = \tilde{\Omega}(\epsilon_O^{-2}), \quad (42)$$

and the total evolution time

$$T_{\text{total}} = \tilde{\mathcal{O}}(NL T_{\max}) = \tilde{\mathcal{O}}(\Delta^{-1} \epsilon_O^{-2}). \quad (43)$$

It is instructive to contrast the generalized eigenvalue problem in [Eq. \(36\)](#) with that used in quantum subspace methods for eigenvalue estimation [\[30–37\]](#). According to the analysis in [\[34, Theorem 2.7\]](#), if each entry of the projected Hamiltonian and overlap matrices is estimated using  $N_s$  samples, then the statistical error per entry scales as  $\mathcal{O}(N_s^{-1/2})$ . The corresponding error in the eigenvalue of interest scales as  $\mathcal{O}(N_s^{-1/(2(1+\alpha))})$ , where  $0 \leq \alpha \leq \frac{1}{2}$  arises from a weighted geometric mean inequality for the projected matrices. Thus, the overall convergence can be slower than the standard shot-noise-limited scaling  $\mathcal{O}(N_s^{-1/2})$  whenever  $\alpha > 0$ . Moreover, the total error is further amplified by a factor of  $\text{poly}(D)$ , where  $D$  denotes the dimension of the subspace. In practice,  $D$  is typically kept small to mitigate this amplification. In our setting, however,  $D$  is approximately  $\max(L, R)$  multiplied by the number of  $\{t_n\}$ 's, which is usually very large. Our error bound, in contrast, is largely insensitive to this subspace dimension. We can even afford to measure each experiment indexed by  $t_n$  once and still achieves the shot-noise-limited scaling. This robustness arises because the singular value truncation in [Eq. \(34\)](#) ensures that the right-hand side of [Eq. \(36\)](#) is well conditioned, thereby avoiding the instability caused by inverting ill-conditioned overlap matrices and reducing the sample complexity.

## VI. ANCILLA-FREE ALTERNATIVE TO THE GENERALIZED HADAMARD TEST

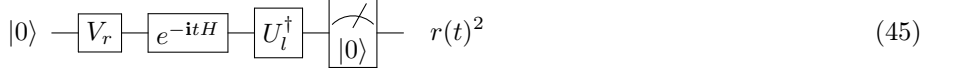
In the QFAMES algorithm, the generalized Hadamard test circuits [Eq. \(13\)](#) and [Eq. \(29\)](#) are used to generate the quantum data  $Z_{l,r,n}$ , and for observables,  $Z_{l,r,n,n'}^O$ , which requires controlled Hamiltonian evolution and initial state preparation circuits. Such controlled operations can be challenging to implement on near-term and even early fault-tolerant quantum devices. To address this limitation, several alternatives to the generalized Hadamard test have recently been proposed that are either ancilla-free [\[6–8, 10, 47\]](#), or substantially reduce requirements of controlled operations [\[9\]](#). The method in [\[6\]](#) is particularly suitable for QFAMES, as it

1. exactly allows to measure  $Z_{l,r,n} = \langle \phi_l | e^{-iHt_n} | \psi_r \rangle$  with different left and right initial states  $|\phi_l\rangle$  and  $|\psi_r\rangle$ ;
2. can produce the data for  $t$  in the time interval  $[0, \sigma T]$  in a single execution of the algorithm;
3. can be easily generalized to the cases involving multiple time evolutions, thereby allowing access to the 4-tensor  $Z_{l,r,n,n'}^O$  in the observable version of QFAMES.

Below we will briefly introduce this algorithm. A key observation is that the main difficulty of measuring  $Z_{l,r,n} = r(t_n) e^{i\phi(t_n)}$  lies in the phase  $\phi(t_n)$  rather than the absolute value  $r(t_n)$ , and these two quantities are related via complex analysis. Notice that for a bounded Hamiltonian, the analytic continuation  $Z_{l,r}(z) = \langle \phi_l | e^{-iHz} | \phi_r \rangle$  is a holomorphic function on the complex plane  $z = t - i\beta$ , and so is  $\ln Z_{l,r}(z) = \ln r(z) + i\phi(z)$  when  $Z_{l,r}(z) \neq 0$ . Therefore, the Cauchy-Riemann equation connects the absolute value and phase as

$$\frac{d\phi(t)}{dt} = \frac{\partial \phi(z)}{\partial t} \bigg|_{\beta=0} = \frac{\partial \ln r(z)}{\partial \beta} \bigg|_{\beta=0} \approx \frac{1}{2h} [\ln r(t - ih) - \ln r(t + ih)]. \quad (44)$$

The last step is the finite difference approximation and  $h$  is a small constant. Assuming knowledge of  $\phi(0)$ , one can obtain the phases  $\phi(t)$  for  $t$  in the desired interval by integrating Eq. (44). Thus it is only required to measure the quantities  $r(t) = |\langle \phi_l | e^{-iHt} | \psi_r \rangle|$  and  $r(t \pm ih) = |\langle \phi_l | e^{-iHt} e^{\pm ihH} | \psi_r \rangle|$ . The corresponding circuits are



$$|0\rangle \xrightarrow{V_r} \xrightarrow{e^{\pm ihH}/c_{\psi_r, \pm}} \xrightarrow{e^{-itH}} \xrightarrow{U_l^\dagger} \xrightarrow{\text{Measurement}} r(t \pm ih)^2 / c_{\psi_r, \pm}^2 \quad (46)$$

In addition to the necessary state preparations and real-time evolutions, these circuits require at most *a single short step* of imaginary time evolution to one side of the initial states, and the last step is a projective measurement onto computational basis state  $|0\rangle$ .

Note that the imaginary time evolution is non-unitary and thus a pre-computed normalization factor  $c_{\psi_r, \pm} = \sqrt{\langle \psi_r | e^{\pm 2hH} | \psi_r \rangle}$  is required in the quantum circuit. When the initial state  $|\psi_r\rangle = V_r |0\rangle$  has short correlation length and the Hamiltonian  $H$  is local, the single step of imaginary time evolution can be approximated by local unitary evolution operators times  $c_{\psi_r, \pm}$ , as shown in the quantum imaginary time evolution (QITE) algorithm [41]. If it is not the case, there also exist alternatives to QITE. For example, one can introduce a single auxiliary qubit to implement the single step imaginary-time evolution via probabilistic imaginary-time evolution (PITE) algorithms [42, 48], while still avoiding the requirement for controlled long real-time evolutions.

To measure  $Z_{l,r}^O(t, t')$ , we just need to view  $t$  and  $t'$  as two separate variables and perform the algorithm from both sides. The modified circuits are as follows:

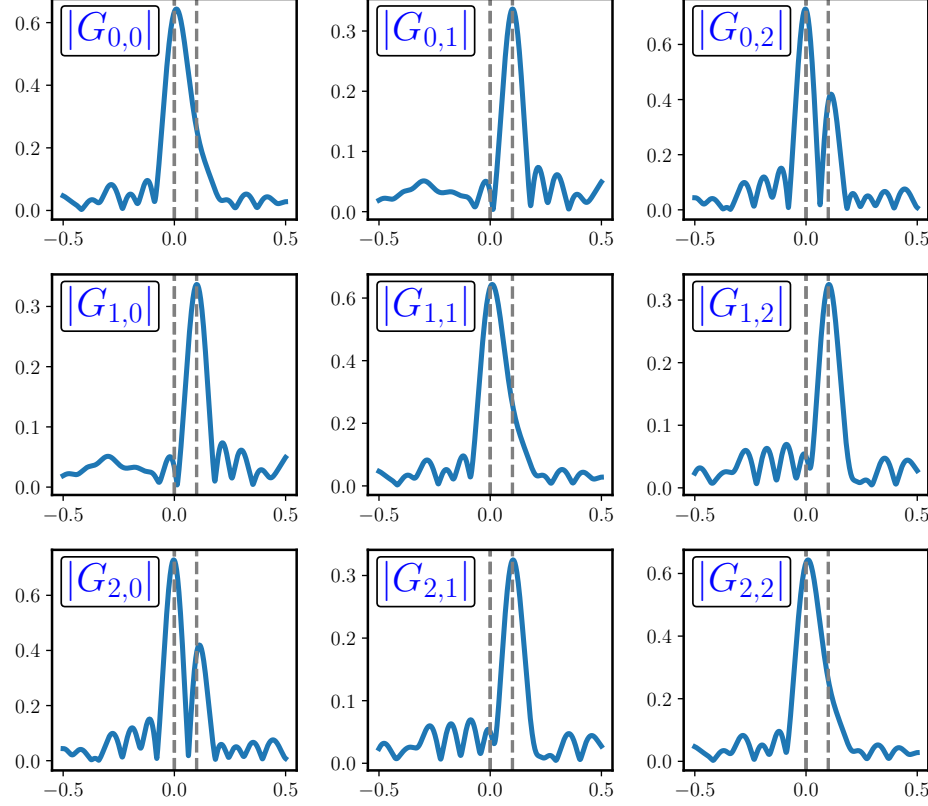
$$|0\rangle \xrightarrow{V_r} \xrightarrow{e^{-itH}} \xrightarrow{O} \xrightarrow{e^{it'H}} \xrightarrow{U_l^\dagger} \xrightarrow{\text{Measurement}} |Z_{l,r}^O(t, t')|^2 \quad (47)$$

$$|0\rangle \xrightarrow{V_r} \xrightarrow{\frac{e^{\pm hH}}{c_{\psi_r, \pm}}} \xrightarrow{e^{-itH}} \xrightarrow{O} \xrightarrow{e^{it'H}} \xrightarrow{U_l^\dagger} \xrightarrow{\text{Measurement}} |Z_{l,r}^O(t \pm ih, t')|^2 / c_{\psi_r, \pm}^2 \quad (48)$$

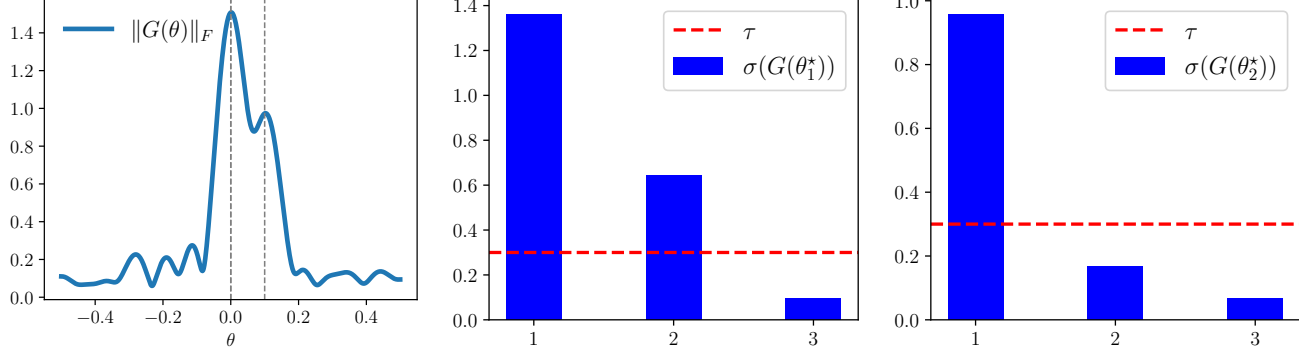
$$|0\rangle \xrightarrow{V_r} \xrightarrow{e^{-itH}} \xrightarrow{O} \xrightarrow{e^{it'H}} \xrightarrow{\frac{e^{\pm hH}}{c_{\phi_l, \pm}}} \xrightarrow{U_l^\dagger} \xrightarrow{\text{Measurement}} |Z_{l,r}^O(t, t' \pm ih)|^2 / c_{\phi_l, \pm}^2 \quad (49)$$

## VII. NUMERICAL RESULTS

In this section, we numerically demonstrate the efficiency of QFAMES by applying it to three models: (1) A simple illustrative example in Section VII A; (2) A transverse Field Ising model (TFIM) in Section VII B; (3) 2D Toric code example in Section VII C. For simplicity, we set the left and right initial states to be the same. In the first case, we provide three simple initial states that are not orthogonal to each other to estimate the multiplicity of ground state energy. For the TFIM, we take five low-energy matrix product states with bond dimension 2 as the initial states. We not only compute the ground state degeneracies, but also probe ground state properties of different quantum phases by measuring observable expectation values. In the third example, we employ an increasing number of random initial states to estimate the ground-state degeneracy of a model with topological order, thereby demonstrating that QFAMES is applicable in a broad range of settings.



(a)



(b)

(c)

(d)

Figure 3: Illustration of the QFAMES algorithm on the illustrative example. The dashed vertical lines are the locations of the eigenvalues. (a): The magnitude of  $G_{i,j}(\theta) = \frac{1}{N} \sum_{n=1}^N Z_{i,j,n} e^{i\theta t_n}$  for each  $0 \leq i, j \leq 2$ . The gray dashed lines indicate the positions of the eigenvalues. (b): The Frobenius norm  $\|G(\theta)\|_F$ , which clearly identifies the two distinct dominant eigenvalues. (c) and (d): The singular values of  $G(\theta)$  at each  $\lambda_i^*$ , accurately indicating the corresponding multiplicities when the threshold  $\tau = 0.1\sqrt{LR} = 0.3$ .

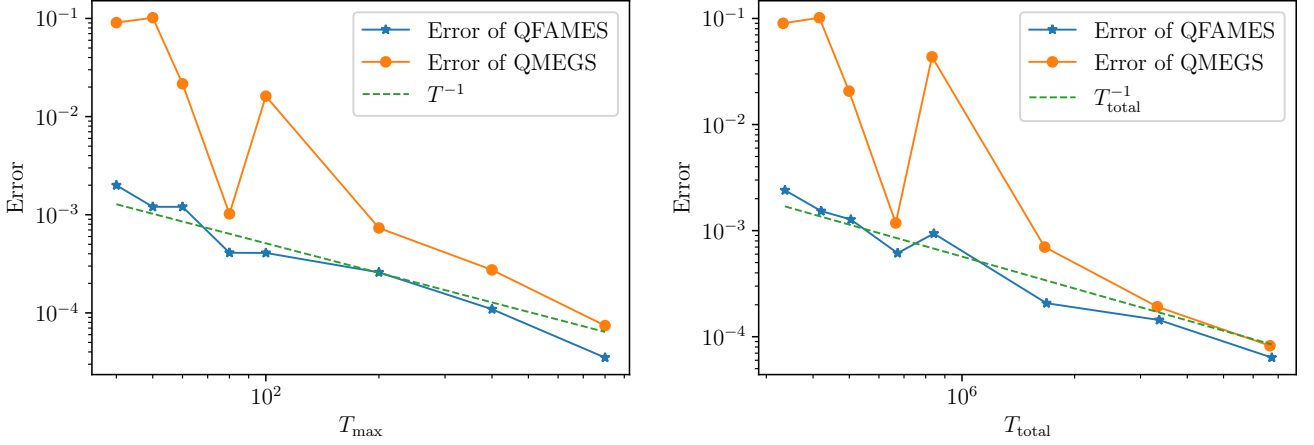


Figure 4: QFAMES (Algorithm 1) vs QMEGS in the illustrative example as a function of (left): max evolution time  $T_{\max} = \sigma T$ , and (right): total evolution time  $T_{\text{total}}$ . The dashed line stands for the fitted error proportional to  $1/T$ , as predicted by Eq. (27).

### A. Illustrative example

To illustrate the effectiveness of QFAMES, we consider a simple Hamiltonian with three eigenvalues:  $\lambda_0 = \lambda_1 = 0$  and  $\lambda_2 = 0.1$ . There are only two distinct eigenvalues:  $\lambda_0^* = 0$  and  $\lambda_1^* = 0.1$ . The Hamiltonian is given by

$$H = \begin{bmatrix} 0 & 0 & 0 \\ 0 & 0 & 0 \\ 0 & 0 & 0.1 \end{bmatrix}, \quad (50)$$

and we assume access to three initial states  $|\phi_0\rangle, |\phi_1\rangle, |\phi_2\rangle$  with overlap matrix:

$$\Phi = \Psi = \frac{1}{\sqrt{3}} \begin{bmatrix} 1 & 1 & 1 \\ 1 & -1 & 1 \\ 1 & 1 & -1 \end{bmatrix}. \quad (51)$$

In this case, the tail overlap  $p_{\text{tail}} = 0$  and all eigenvalues are dominant. A single initial state approach would only yield an estimate of the location of  $\lambda_0^*$  and  $\lambda_1^*$  but fail to resolve the degeneracy of  $\lambda_0^*$ . Moreover, because the overlaps with  $\lambda_2$  are not sufficiently dominant compared to those with  $\lambda_0, \lambda_1$ , single-state approaches might not reliably estimate the location of  $\lambda_2$ .

To resolve the degeneracy at  $\lambda_0^*$ , it is essential to utilize the off-diagonal entries of the data tensor, which encode important information about the spectral structure. We can check that the  $\mathcal{Z}$  matrix has the form

$$\mathcal{Z}(t) = \frac{1}{3} \begin{bmatrix} 2 + e^{-\text{i}0.1t} & e^{-\text{i}0.1t} & 2 - e^{-\text{i}0.1t} \\ e^{-\text{i}0.1t} & 2 + e^{-\text{i}0.1t} & -e^{-\text{i}0.1t} \\ 2 - e^{-\text{i}0.1t} & -e^{-\text{i}0.1t} & 2 + e^{-\text{i}0.1t} \end{bmatrix}. \quad (52)$$

The off-diagonal entry  $\mathcal{Z}_{0,1}(t) = e^{-\text{i}0.1t}$ , for example, reveals two key pieces of information:

1.  $\lambda_3 = 0.1$  must be one of the dominant eigenvalues, as it is the only effective frequency present in the signal;
2. The degeneracy of dominant eigenvalue  $\lambda_0^*$  must be at least two, since the signal corresponding to the frequency  $\lambda \approx 0$  vanishes in this off-diagonal entry.

The first point allows for a more accurate estimation of the location of  $\lambda_2$ , while the second provides insight into the multiplicity of  $\lambda_0^*$ .

Now we perform numerical simulations to demonstrate the main ideas of QFAMES. We independently sample  $\{t_n\}_{n \in N}$  with  $N = 2000$  from the truncated Gaussian distribution  $a_T(t)$  defined in Eq. (16) with truncation parameter  $\sigma = 1$ , and generate each  $Z_n$  using a single-shot generalized Hadamard test. In Fig. 3(a), we plot the magnitude of each entry of  $G(\theta)$  for  $T = 40$ . The diagonal entries exhibit a prominent peak corresponding to  $\lambda_0^*$ , while the second

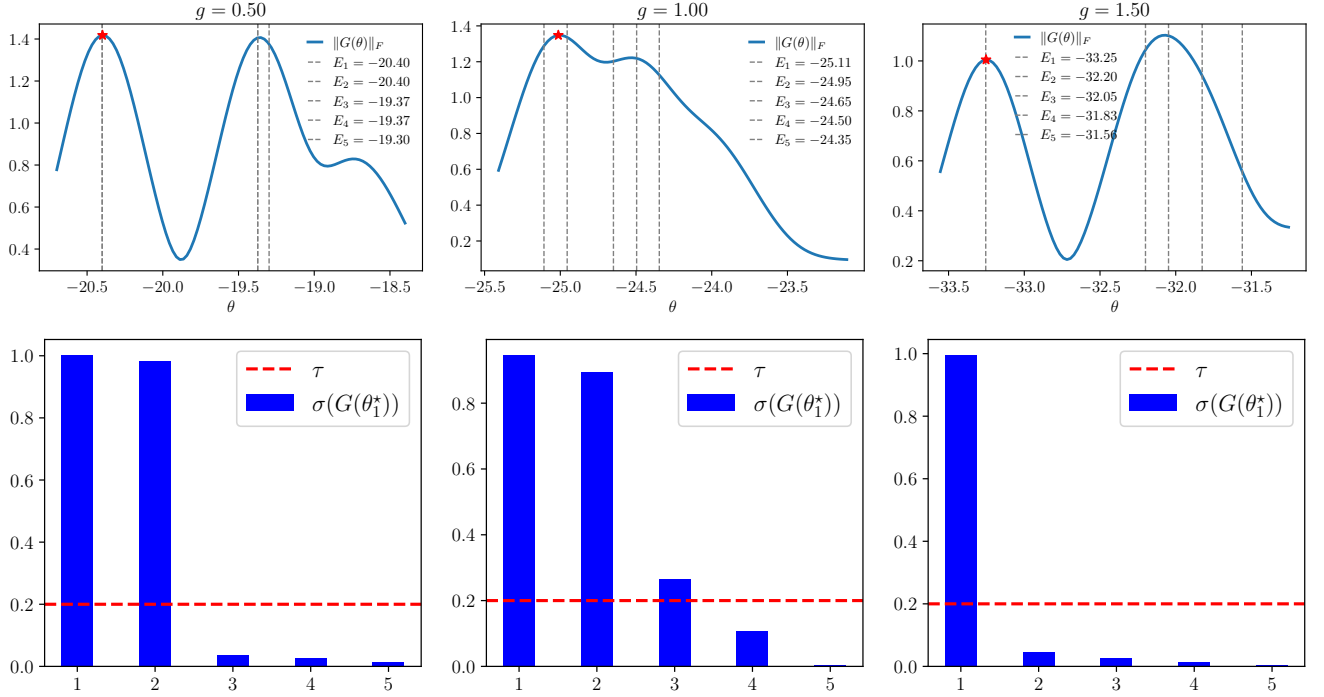


Figure 5: Illustration of the QFAMES algorithm on the TFIM model. The upper row shows the Frobenius norm of  $G(\theta)$  around the ground state energy for  $g = 0.5, 1.0$  and  $1.5$ , from left to right. The dashed lines stand for the 5 lowest lying energy eigenvalues. The lower row shows the singular values of the  $G(\theta_1^*)$ , where  $\theta_1^*$  is the leftmost peak found in corresponding Frobenius norm (marked with red stars). The SVD cutoff threshold is set to be 0.2.

peak near  $\lambda_2$  is not clearly identifiable. As a result, the standard QPE based approach described in Section A cannot locate  $\lambda_2$  and fails to reveal the multiplicity of  $\lambda_0^*$ . Although the diagonal landscapes are the same in Fig. 3(a), if we focus on the off diagonal landscapes, it is evident that there exists one dominant eigenvalue near  $\lambda_2 = 0.1$ . This can be more systematically observed in the plot of the Frobenius norm  $\|G(\theta)\|_F^2$  in Fig. 3(b), which clearly reveals two distinct dominant eigenvalues, including an ‘‘amplified’’ peak near  $\lambda_0 = \lambda_1 = 0$ . Figures Fig. 3(c) and Fig. 3(d) show the singular values of  $G(\theta)$  at  $\theta = 0$  and  $\theta = 0.1$ , respectively. They exactly recover the multiplicities: two dominant eigenvalues near zero and one near 0.1.

In Fig. 4, we show the accuracy of the QFAMES algorithm in locating dominant eigenvalues as a function of  $T$ . The parameters are chosen as follows: SVD threshold  $\tau = 0.1\sqrt{LR}$ , block parameter  $\alpha = 5$ , search parameter  $q = 0.005$ , and  $T$  takes values 40, 50, 60, 80, 100, 200, 400, and 800. The error is defined as:

$$\text{Error} = \max_i |\theta_i^* - \lambda_i^*|. \quad (53)$$

In Fig. 4, we also include a comparison with the QMEGS algorithm [23], using the same parameters as QFAMES except for  $N = 6000$ , which ensures the total number of Hamiltonian simulations is the same. From the graph, we observe that QFAMES achieves significantly lower error than QMEGS when  $T_{\max} < 100$ , while the errors of both methods become comparable for larger  $T_{\max}$ . This demonstrates the advantage of QFAMES in identifying dominant eigenvalues when  $T_{\max}$  is not sufficiently large, aided by the use of off-diagonal entries in  $G(\theta)$ . Furthermore, we note that QMEGS cannot identify the multiplicity of  $\lambda_0^*$ , as it relies solely on the diagonal entries of  $G(\theta)$ , whereas QFAMES accurately estimates the multiplicities of both dominant eigenvalues.

## B. Transverse Field Ising Model (TFIM)

Here we consider the transverse field Ising model on a spin chain of length  $L$ :

$$H = - \sum_{i=1}^{L-1} Z_i Z_{i+1} - g \sum_{i=1}^L X_i, \quad (54)$$

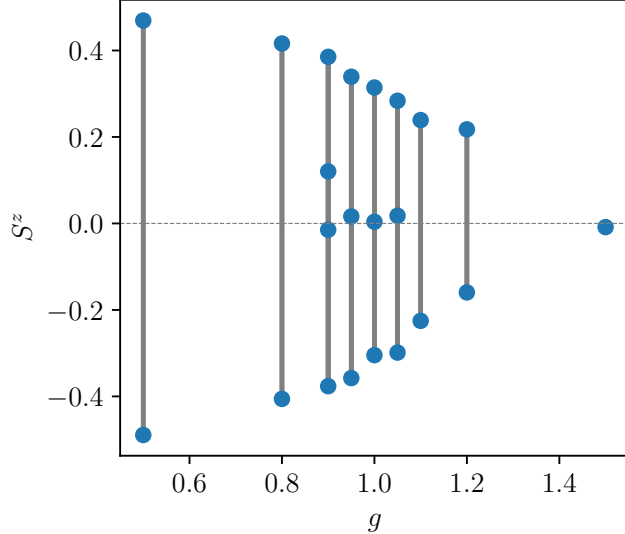


Figure 6: Illustration of [Algorithm 2](#) on the TFIM model. The observable is  $S^z = \frac{1}{2L} \sum_{i=1}^L Z_i$ . In the manifold of near-ground-state cluster, the possible ranges of observable expectation values are shown by the gray lines. A transition from ferromagnetic to paramagnetic phase can be observed when  $g$  increases from 0.5 to 1.5.

where  $Z_i$  and  $X_i$  are the Pauli operators acting on the  $i$ -th qubit and  $g$  is the coupling coefficient. The ground state of the TFIM lies in the ferromagnetic phase for  $g < 1$ , and undergoes a quantum phase transition at  $g = 1$  to the paramagnetic phase for  $g > 1$ . Note that the GSD is 2 in the ferromagnetic phase, 1 in the paramagnetic phase, and system is is gapless at the phase transition point.

In our test, we set system size  $L = 20$  and  $g = 0.5, 0.8, 0.9, 0.95, 1, 1.05, 1.1, 1.2, 1.5$ . For each  $g$ , the set of initial states are chosen to be 5 matrix product states (MPS) of bond dimension 2 that are orthogonal to each other and have approximately lowest energies, and we simulate the time evolutions with time-evolving block decimation (TEBD) algorithm [49] with maximum MPS bond dimension  $\chi = 100$ . The sample parameters are  $N = 10^4$ <sup>ii</sup> and  $T/\sqrt{2} = 2.5$ . In [Fig. 5](#) we demonstrate how QFAMES can be applied to resolve the ground state degeneracy of TFIM. When  $g = 0.5$ , we can clearly see a GSD of 2. When  $g = 1$ , we are in the gapless phase, and more states around the ground state are detected with a moderate choice of  $T$ . While when  $g = 1.5$ , the ground state is found to be unique.

We can further obtain the ground state properties of each phase by applying [Algorithm 2](#). The observable we choose is

$$S^z = \frac{1}{2L} \sum_{i=1}^L Z_i \quad (55)$$

and the results are illustrated in [Fig. 6](#). When  $g = 0.5$ , the solutions to the generalized eigenvalue problem, which serve as an estimation of eigenvalues of  $(\langle E_k | S^z | E_{k'} \rangle)_{k, k' \in [m_i]}$ , are close to  $\pm 0.5$ , showing the ground states lie in the ferromagnetic phase. As  $g$  increases, the possible range of expectation values of  $S^z$  in the near-ground-state cluster manifold reduces and finally reaches 0 at  $g = 1.5$ , corresponding to the paramagnetic phase.

### C. 2D Toric Code

In many-body systems, GSD is a hallmark of topological order and depends only on the global topology of the system. For stabilizer Hamiltonians, the GSD is exactly  $2^k$ , where  $k$  is the number of logical qubits encoded by the code. In this section, we estimate the ground-state degeneracy of the 2D Toric code Hamiltonians [50] as an example.

<sup>ii</sup> For simulation simplicity, for the time parameters  $t_n$  and  $t'_n$  in [Eq. \(30\)](#), we choose  $(t_n, t'_n) \in \mathcal{T}_{\text{sample}} \times \mathcal{T}_{\text{sample}}$ , where  $\mathcal{T}_{\text{sample}}$  consist of  $\sqrt{N} = 100$  samples drawn from Gaussian density distribution  $a_{T/\sqrt{2}}(t)$ .

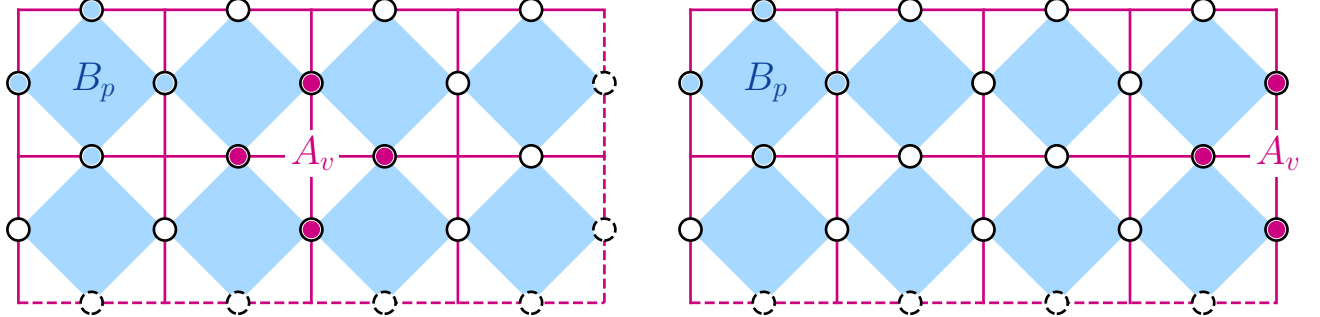


Figure 7: 2D Toric codes on a 2-by-4 lattice with (left) torus, and (right) cylinder boundary conditions. Dashed lines stand for periodic boundary conditions in the corresponding directions. The models consist of 16 and 18 qubits, respectively, represented by the small circles.

The Toric code ground state is known to exhibit  $\mathbb{Z}_2$  topological order, which has been realized on a quantum computer based on the prior knowledge of its explicit form [51]. In contrast, our numerical experiment starts with a collection of random initial states. Specifically, the Toric code Hamiltonian on a 2D lattice is given by

$$H = - \sum_v A_v - \sum_p B_p, \quad (56)$$

where  $v$  denotes the vertices and  $p$  the plaquettes of the lattice. Qubits live on the edges, with  $i \in v$  labeling the edges touching a vertex  $v$ , and  $i \in p$  labeling the edges surrounding a plaquette  $p$ . The corresponding stabilizer operators are  $A_v = \prod_{i \in v} X_i$  and  $B_p = \prod_{i \in p} Z_i$ . We study the Toric code model on a 2-by-4 lattice with torus and cylinder boundary conditions, as demonstrated in Fig. 7. Their GSDs are *four* and *two*, respectively. The numerical experiment proceeds as follows:

1. We randomly sample vectors from the Haar distribution and apply imaginary-time evolution  $\exp(-\beta H)$  to enhance their overlap with the ground-state subspace.
2. We then apply QFAMES to these boosted vectors to estimate the multiplicity of the cluster corresponding to the smallest eigenvalue.

We find that in the first step of the algorithm, it is necessary to generate a sufficient number of initial states such that the ground-state subspace is contained within their linear span. This condition is essential for correctly estimating the ground-state multiplicity. We also remark that imaginary-time evolution is generally not efficient for large-scale, general Hamiltonians on a quantum computer, and is used here primarily for illustrative purposes. In practical applications, one would need to employ more quantum-friendly methods for generating random low-energy states.

We use  $N = 300$  samples, and set circuit depth parameter  $T = 10$ , the Gaussian truncation parameter  $\sigma = 1$ , and SVD threshold  $\tau = \sqrt{LR}/15 = L/15$ . For inverse temperature  $\beta$  and the number of states  $L$ , we consider different configurations:  $(\beta = 10, L = 15)$  and  $(\beta = 10, L = 25)$ , and  $(\beta = 15, L = 15)$ . Each setup is repeated 10 times, and the averaged singular values are output. Results are shown in Fig. 8. Four and two large singular values can respectively be identified for the two boundary conditions. The performance of the algorithm is also shown to be enhanced by (1) increasing the number of initial states  $L$  (the second column in Fig. 8 compared with the first one), which strengthens the uniform overlap condition, (2) or increasing the imaginary evolution time  $\beta$  (the third column compared with the first one), which reinforces the sufficient dominance condition in Eq. (4).

## VIII. DISCUSSION

We presented QFAMES, a quantum spectral filtering framework that estimates dominant eigenvalues and their multiplicities by jointly processing cross-correlations from multiple initial states. By exploiting off-diagonal information through generalized Hadamard tests, QFAMES recovers spectral structures that are inaccessible to single-state phase estimation and extends naturally to observable estimation within identified clusters. The algorithm admits rigorous efficiency guarantees.

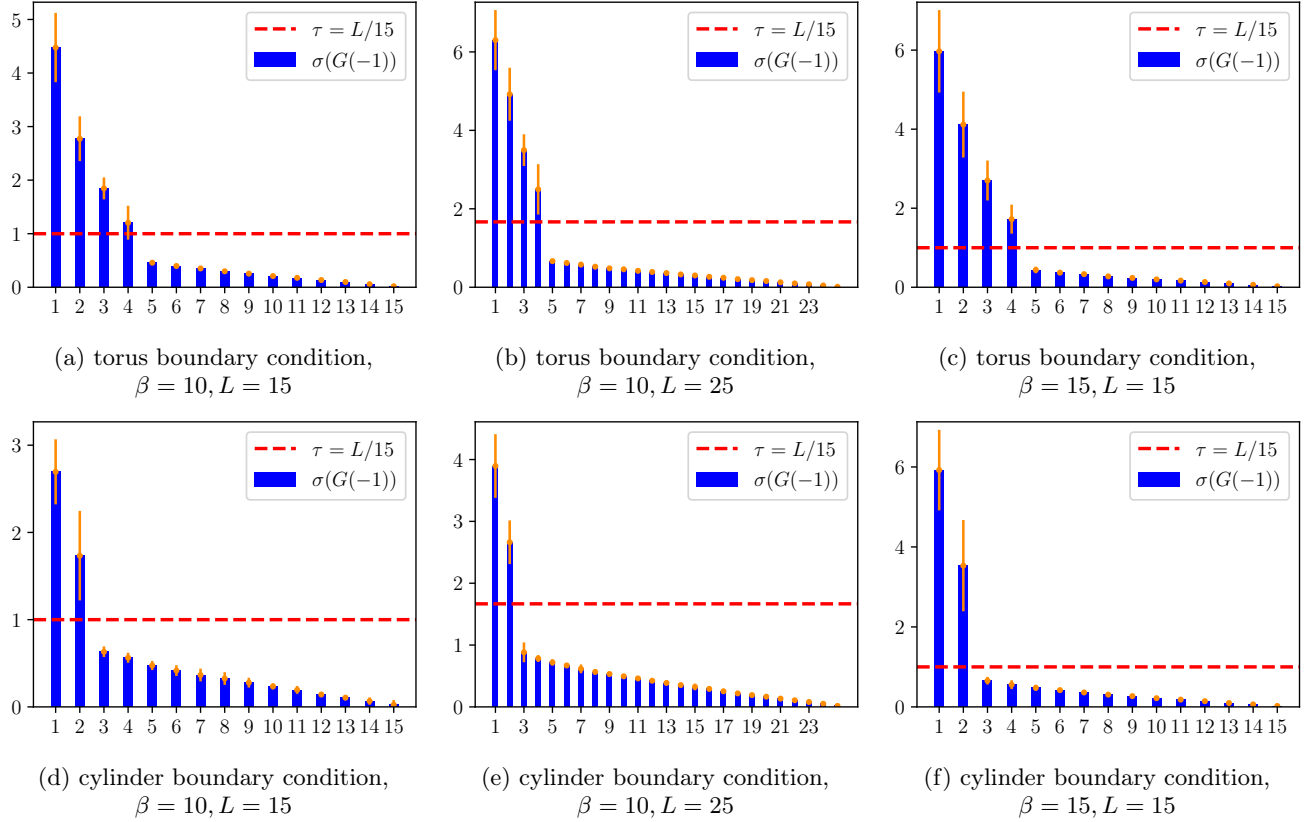


Figure 8: Illustration of GSD estimation for 2D Toric code models with **(upper)** torus and **(lower)** cylinder boundary conditions. The spectra are rescaled to  $[-1, 1]$  and we plot the averaged singular values of  $G(-1)$ . The orange lines are the error bars over 10 trials for each parameter configuration. Four and two large singular values can be clearly identified, respectively. In the second column, we increase the number of initial states  $L$  compared with the first column. In the third column, we increase the imaginary evolution time  $\beta$ .

The quantum data produced by QFAMES naturally form an order-3 tensor. One could attempt to solve the DODS problem using general tensor-decomposition techniques [52–57] or approaches tailored to high-order time series [58, 59]. However, to the best of our knowledge, none of these algorithms provide provable efficiency guarantees in the high-noise or overcomplete regime, and it remains unclear how to extend the existing theoretical results to this setting. In contrast, our analysis gives a simple estimator that is tailored to the QFAMES tensor structure, yields provable efficiency and robustness to measurement noise, and provides exact multiplicity recovery under the stated assumptions. We expect these ideas to be useful beyond the present setting.

The QFAMES algorithm has broad potential applications. For instance, it can be employed to probe the ground-state manifolds of models with topological orders that are difficult to analyze with classical algorithms, such as those exhibiting the fractional quantum Hall effect [60, 61]. In addition, (approximate) degeneracies in the energy spectrum often serve as hallmarks of quantum ergodicity breaking, such as in many-body localization [62, 63] and quantum scars [64–66], and QFAMES provides a practical framework for investigating such phenomena. These examples, together with the short circuit depth nature and ancilla-free implementation of the algorithm, highlight the versatility of QFAMES as a general and efficient tool for uncovering spectral properties across diverse quantum systems, in particular on early fault-tolerant devices.

## ACKNOWLEDGMENTS

This work was supported in part by the U.S. Department of Energy, Office of Science, National Quantum Information Science Research Centers, Quantum Systems Accelerator (Z.D., L.L.), and by the U.S. Department of Energy, Office of Science, Accelerated Research in Quantum Computing Centers, Quantum Utility through Advanced Computational Quantum Algorithms, grant no. DE-SC0025572 (Y.Y., L.L.). L.L. is a Simons Investigator in Mathematics. We thank

Wendy Billings, Dominik Hangleiter, Martin Head-Gordon and Birgitta Whaley for helpful discussions.

## NOMENCLATURE

$[n]$	The index set $\{0, 1, \dots, n - 1\}$
<b>Hamiltonian notations</b>	
$H = \sum_{m \in [M]} \lambda_m  E_m\rangle \langle E_m $	Hamiltonian of interest and its spectral decomposition
$\mathcal{D} \subset [M]$	Index set of dominant eigenvalues
$I \in \mathbb{N}_+$	The number of distinct dominant eigenvalues
$\{\lambda_i^*\} \subset \mathbb{R}$	The distinct dominant eigenvalues
$\mathcal{D}_i \subset \mathcal{D}$	The index set of dominant eigenvectors with eigenvalue $\lambda_i^*$
$\Delta \in \mathbb{R}_+$	The minimum separation between distinct dominant eigenvalues
<b>Initial states notations</b>	
$L, R \in \mathbb{N}_+$	Number of initial states
$\{U_l\}_{l \in [L]}, \{V_r\}_{r \in [R]}$	Initial state preparation unitaries
$\{ \phi_l\rangle\}_{l \in [L]}, \{ \psi_r\rangle\}_{r \in [R]}$	Initial states prepared by $U_l$ and $V_r$
$\Phi \in \mathbb{C}^{L \times M}$	Overlaps between $\{ \phi_l\rangle\}$ and $\{ E_m\rangle\}$
$\Psi \in \mathbb{C}^{R \times M}$	Overlaps between $\{ \psi_r\rangle\}$ and $\{ E_m\rangle\}$
$p_{\text{tail}} \in \mathbb{R}$	Total overlaps with the non-dominant eigenvectors
$p_{\min} \in \mathbb{R}$	Minimum overlap with a dominant eigenvector
$\chi \in \mathbb{R}_+$	Uniform overlap condition parameter
<b>Hamiltonian evolution times notations</b>	
$N \in \mathbb{N}_+$	Number of evolution times
$\{t_n\}_{n \in [N]} \subset \mathbb{R}$	Evolution time samples
$a_T^{\text{trunc}}(t)$	Probability density function (PDF) of the truncated Gaussian distribution
$F(x)$	Fourier transform of $a(t)$ ; $F(x) = \int_{-\infty}^{\infty} e^{ixt} a(t) dt$
$T \in \mathbb{R}$	Circuit depth parameter
$\sigma \in \mathbb{R}$	Gaussian truncation parameter such that $a_T(t)$ is supported over $[-\sigma T, \sigma T]$
<b>Tensor notations</b>	
$Z \in \mathbb{C}^{L \times R \times N}$	Data tensor collected from the measurement outcomes for DODS estimation
$Z_n \in \mathbb{C}^{L \times R}$	A slice of $Z$ defined as $Z_{:, :, n}$
$G(\theta) \in \mathbb{C}^{L \times R}$	The contraction of $Z$ along the third coordinate with the vector $(e^{i\theta t_n})_{n \in [N]}$
$Z^O \in \mathbb{C}^{L \times R \times N}$	Data tensor collected from the measurement outcomes for observable estimation
$G^O(\theta) \in \mathbb{C}^{L \times R}$	The contraction of $Z^O$ along the third coordinate
<b>Algorithm notations</b>	
$q \in \mathbb{R}$	The grid-search parameter such that the grid width is $q/T$

$J \in \mathbb{N}_+$	The number of grid points
$\{\theta_j\} \subset \mathbb{R}$	The grid points
$\alpha \in \mathbb{R}$	Width of the block
$\{\mathcal{B}_i\}$	Blocked grid points around each peak
$\eta \in [0, 1]$	The success probability of the algorithm
$\tilde{I} \in \mathbb{N}_+$	Estimated number of distinct dominant eigenvalues
$\{\theta_j^*\}_{i \in [\tilde{I}]} \subset [-\pi, \pi]$	Estimated dominant eigenvalues
$\tau \in \mathbb{R}$	The threshold for the singular values
$\{m_i\} \subset \mathbb{N}_+$	Estimated multiplicities

### Appendix A: Quantum phase estimation and limitation

The standard quantum phase estimation (QPE) algorithm estimates eigenvalues of a Hamiltonian  $H$  by applying the quantum Fourier transform (QFT) to an initial state. Recently, a class of “post-Kitaev” phase estimation algorithms (see e.g., [19–23, 25, 26]) has been proposed for early fault-tolerant quantum computers. These algorithms build upon the original single-ancilla Kitaev algorithm [16], which utilizes the output from the Hadamard test circuit. However, they differ in their strategies for selecting Hamiltonian simulation times and in their use of advanced classical signal processing techniques to handle quantum noisy data.

Unlike QFT-based algorithms, post-Kitaev methods require only a single ancilla qubit while still achieving Heisenberg-limited scaling. Moreover, they are capable of simultaneously estimating *multiple* eigenvalues, making them particularly advantageous for early fault-tolerant quantum devices. We first briefly review the structure of post-Kitaev phase estimation algorithms, which can be organized within the following three-step framework:

1. Generate a sequence of real numbers  $\{t_n\}_{n \in [N]}$  as the Hamiltonian evolution times.
2. Apply Hadamard test circuit (Fig. 9) to the initial state  $|\phi\rangle$  for each time  $t_n$ , and collect the measurement outcomes to form a dataset  $\{(t_n, Z_n)\}_{n \in [N]}$ , where  $Z_n \in \{\pm 1 \pm \mathbf{i}\}$ .
3. Perform classical post-processing on the dataset  $\{(t_n, Z_n)\}_{n \in [N]}$  to estimate the dominant eigenvalues  $\{\lambda_m\}_{m \in \mathcal{D}}$ .

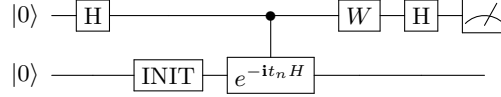


Figure 9: Hadamard test circuit.  $W$  is either the identity or the phase gate  $S^\dagger$ . Here INIT  $|0\rangle = |\phi\rangle$ .

For each  $n$ , the Hadamard test circuit guarantees that

$$\mathbb{E}[Z_n] = \langle \phi | e^{-\mathbf{i}Ht_n} | \phi \rangle = \sum_{m \in [M]} \underbrace{|\langle \phi | E_m \rangle|^2}_{:= p_m} \cdot e^{-\mathbf{i}\lambda_m t_n}. \quad (\text{A1})$$

Thus, the dataset  $\{(t_n, Z_n)\}_{n \in [N]}$  corresponds to the unbiased noisy samples of the Fourier signal

$$x(t) = \sum_{m \in [M]} p_m \exp(-\mathbf{i}\lambda_m t). \quad (\text{A2})$$

Estimating the dominant eigenvalues  $\{\lambda_m\}_{m \in \mathcal{D}}$  from these samples is then equivalent to the classical spectral estimation problem, which has been extensively studied in signal processing. Different post-Kitaev phase estimation algorithms primarily vary in the choice of  $t_n$  in the first step and the classical spectral estimation technique used in the

third step to extract the dominant eigenvalues  $\{\lambda_m\}_{m \in \mathcal{D}}$  from these samples. Examples include complex exponential least squares [21, 22, 24], robust phase estimation [27], Gaussian filtering and searching [23, 28], ESPRIT [29, 67], compressed sensing [25, 26], to name a few.

Theoretical analyses have demonstrated that state-of-the-art post-Kitaev algorithms can achieve Heisenberg-limited scaling. Specifically, for a target precision  $\epsilon$ , the total Hamiltonian evolution time required scales as  $1/\epsilon$ , ensuring that the algorithm estimates each dominant eigenvalue to within  $\epsilon$ -accuracy [22, 23, 29]. Moreover, these algorithms achieve “short” circuit depths: for well-separated dominant eigenvalues, the maximal evolution time scales as  $p_{\text{tail}}/\epsilon$ . These properties, along with other advantages (see [23]), make post-Kitaev methods particularly suitable for early fault-tolerant quantum devices.

However, QPE and post-Kitaev phase estimation algorithms encounter fundamental limitations when it comes to resolving closely spaced eigenvalues or determining the multiplicities of degenerate eigenvalues. In the nearly degenerate case, although these algorithms guarantee that the output is close to one of the dominant eigenvalues, they cannot distinguish eigenvalues separated by extremely small gaps. For instance, if a Hamiltonian has two dominant eigenvalues with an arbitrarily small separation, the algorithm may return a single estimate that is  $\epsilon$ -close to both, without revealing their multiplicities. In the degenerate case, when access is restricted to a single initial state, these algorithms are incapable of producing the correct multiplicity. This limitation is formalized in [Theorem B.1](#).

## Appendix B: Uniform overlap condition for the QFAMES algorithm

For a matrix  $A \in \mathbb{C}^{m \times n}$  with  $m \geq n$ , denote its singular values as  $\{s_i\}_{i \in [n]}$ . Then we define  $s_{\min}(A) = \min_i s_i$  to be the smallest singular value of  $A$ . We also define

$$s_{\text{avg}}(A) = \sqrt{\frac{\sum_i s_i^2}{n}} = \frac{\|A\|_F}{\sqrt{n}} \quad (\text{B1})$$

to be the average singular value of  $A$ , where  $\|A\|_F$  is the Frobenius norm of  $A$ .

In this section, we formally present the uniform overlap condition for the QFAMES algorithm.

**Assumption 1** (Uniform overlap condition). *For each  $i \in [I]$ , let  $\mathcal{D}_i := \{m \in \mathcal{D} | \lambda_m = \lambda_i^*\}$  denote the index set of dominant eigenvectors with the same eigenvalue  $\lambda_i^*$ . We assume there exists a constant  $\chi > 0$  such that, for every  $i \in [I]$ , the following inequalities hold:*

$$s_{\min}(\Phi_{:, \mathcal{D}_i}) > \frac{s_{\text{avg}}(\Phi_{:, \mathcal{D}_i})}{1 + \chi}, \quad s_{\min}(\Psi_{:, \mathcal{D}_i}) > \frac{s_{\text{avg}}(\Psi_{:, \mathcal{D}_i})}{1 + \chi}. \quad (\text{B2})$$

Recall from [Eq. \(5\)](#) that

$$\min_{|E\rangle \in \mathcal{E}_i, \langle E|E\rangle=1} \sum_{l \in [L]} |\langle \phi_l | E \rangle|^2 = \min_{\|u\|=1} \|\Phi_{:, \mathcal{D}_i} u\|^2 = s_{\min}(\Phi_{:, \mathcal{D}_i})^2. \quad (\text{B3})$$

Then the uniform overlap condition states that the minimal singular value must be  $(1 + \chi)^{-1}$  times larger than the average singular value, for both  $\Phi_{:, \mathcal{D}_i}$  and  $\Psi_{:, \mathcal{D}_i}$ .

The uniform overlap condition implies that  $\Phi_{:, \mathcal{D}_i}$  and  $\Psi_{:, \mathcal{D}_i}$  have full column ranks. The latter is a *necessary* condition for any algorithm to correctly estimate multiplicities. This is summarized in the following proposition. As a corollary, when there is only a single initial state, it is impossible to resolve eigenstate degeneracy in the setting of [Theorem B.1](#), which corresponds the case of QPE and post-Kitaev phase estimation algorithms.

**Proposition B.1** (Information-theoretic indistinguishability). *Assume that we only have access to data produced by the Hadamard test with controlled Hamiltonian evolution  $\exp(-iHt)$  and left and right initial states with overlap matrices  $\Phi$  and  $\Psi$  as defined in [Eq. \(2\)](#). Let  $\mathcal{D}_i$  denote the indices of a degenerate energy eigenvalue subspace. There exists no classical signal-processing algorithm that can reliably determine the multiplicity  $|\mathcal{D}_i|$ , if  $\text{rank}(\Phi_{:, \mathcal{D}_i}) < |\mathcal{D}_i|$  or  $\text{rank}(\Psi_{:, \mathcal{D}_i}) < |\mathcal{D}_i|$ .*

*Proof.* For simplicity, we assume  $\lambda^*$  is the only eigenvalue of  $H$  with degenerate eigenvectors indexed by  $\mathcal{D}$ , meaning  $H = \lambda^* \sum_{m \in \mathcal{D}} |\varphi_i\rangle \langle \varphi_i|$ . According to the assumptions, when the noise is negligible, we have access to quantities of the form

$$\mathcal{Z}_{l,r}(t) = \langle \phi_l | e^{-iHt} | \psi_r \rangle = e^{-i\lambda^* t} \sum_{m \in \mathcal{D}} \Phi_{l,m} \Psi_{r,m}^*. \quad (\text{B4})$$

The corresponding data matrix is  $\Phi\Psi^\dagger$ . If  $\text{rank}(\Phi) = k < |\mathcal{D}|$ , consider the singular value decomposition of  $\Phi = USV^\dagger$ , where the singular values  $s_j = S_{j,j}$  are sorted in a descending order. Therefore  $(\Phi V)_{:,j} = (US)_{:,j} = 0$  for any  $j \geq k$  (assume the column vectors are indexed by  $j \in [|\mathcal{D}|] = \{0, 1, \dots, |\mathcal{D}| - 1\}$ ). Let us take  $\tilde{\Phi} \in \mathbb{C}^{L \times (k+1)}$  and  $\tilde{\Psi} \in \mathbb{C}^{R \times (k+1)}$  defined as

$$\begin{aligned}\tilde{\Phi}_{:,j} &:= (\Phi V)_{:,j}, \quad \tilde{\Psi}_{:,j} := (\Psi V)_{:,j}, \quad \text{for } j \in [k]; \\ \tilde{\Phi}_{:,k} &:= 0, \quad \tilde{\Psi}_{r,k} := \sqrt{1 - \sum_{j \in [k]} |\tilde{\Psi}_{r,j}|^2}, \quad \text{for } r \in [R].\end{aligned}\tag{B5}$$

$\tilde{\Phi}, \tilde{\Psi}$  correspond to the overlap matrices generated by a different Hamiltonian  $\tilde{H}$  that has only multiplicity  $k$  at the dominant eigenvalue  $\lambda^*$ , and an additional eigenvector  $|E_k\rangle$  with a different eigenvalue.  $|E_k\rangle$  is defined to ensure the normalization conditions for the overlap matrices:  $\|\tilde{\Phi}_{l,:}\| = \|\tilde{\Psi}_{r,:}\| = 1$ , for  $l \in [L]$  and  $r \in [R]$ .

Since by construction

$$\tilde{\Phi}\tilde{\Psi}^\dagger = \tilde{\Phi}_{:,[k]}\tilde{\Psi}_{:,[k]}^\dagger = \Phi_{:,\mathcal{D}}VV^\dagger\Psi_{:,\mathcal{D}}^\dagger = \Phi\Psi^\dagger,\tag{B6}$$

we cannot distinguish the signals generated by  $H$  and  $\tilde{H}$ , and hence cannot correctly resolve the multiplicity. The case for  $\text{rank}(\Psi_{:,\mathcal{D}}) < |\mathcal{D}|$  is analogous.  $\square$

In our proof of the main theorem (Theorem C.2), the uniform overlap condition plays an important role in two aspects:

1. In eigenvalue estimation, the condition Eq. (B2) is applied in Eq. (C25) to ensure that

$$\left\| \Phi_{:,\mathcal{D}}(\pi_\theta) (\Psi_{:,\mathcal{D}(\pi_\theta)})^\dagger \right\|_F^2 \quad \text{and} \quad \|\mathcal{G}(\theta \approx \lambda_{\pi_i}^*)\|_F$$

admit sufficiently large lower bounds. This guarantees that the dominant eigenvalues can be detected by identifying the peaks of  $\|\mathcal{G}(\theta)\|_F$ .

2. In multiplicity estimation, the condition ensures that the overlap matrix

$$\Phi_{:,\mathcal{D}\pi_\theta} \left( \Psi_{:,\mathcal{D}\pi_\theta} \right)^\dagger$$

has rank equal to the corresponding degeneracy. This property is then quantitatively exploited in Eq. (C50) to establish a lower bound on the singular values of  $\mathcal{G}(\theta \approx \theta_{\pi_i}^*)$ .

### Appendix C: Rigorous version of Theorem IV.1 and proof

In this section, we introduce and prove a generalized and rigorous version of Theorem IV.1. In the more general setting, we consider the case where each dominant eigenvalue is not exactly degenerate but instead lies within a small interval of width  $\delta$  that is centered at  $\lambda_i^*$ . This motivates the following definition:

**Definition C.1** (Dominant eigenvalue clusters). *There exists parameters  $\Delta \gg \delta > 0$  and  $I \in \mathbb{N}_+$  such that:*

- *The dominant eigenvalues  $\{\lambda_m\}_{m \in \mathcal{D}}$  are covered by  $I$  disjoint cluster intervals  $\{\mathcal{I}_i\}_{i=1}^I$  that are centered at  $\{\lambda_i^*\}_{i=1}^I$ .*
- *Each cluster interval has length at most  $\delta$ .*
- *The cluster intervals are  $\Delta$ -well-separated. That is, for all  $i \neq j \in [I]$ ,  $\text{dis}(\mathcal{I}_i, \mathcal{I}_j) \geq \Delta$ .*

Here,  $I$  is the number of dominant cluster intervals,  $\delta$  is the maximum width of each interval, and  $\Delta$  is the minimum pairwise separation between intervals.

We note that Theorem IV.1 corresponds to the special case  $\delta = 0$ , where each cluster reduces to a single dominant eigenvalue with exact degeneracy. In the more general setting, a dominant eigenvalue cluster may be viewed as an *approximately degenerate* eigenvalue, and our goal is to estimate both the center of each cluster and the number of dominant eigenvalues it contains. (We slightly abuse notation and use  $\lambda_i^*$  to denote the center of the  $i$ -th cluster  $\mathcal{I}_i$ .) The QFAMES algorithm (Algorithm 1) applies directly to this case.

We are now ready to state a generalized and rigorous version of Theorem IV.1:

**Theorem C.2** (General version of Theorem IV.1). *Suppose Assumption 1 hold with  $\chi = \mathcal{O}(1)$ , and the dominant eigenvalue cluster length parameter  $\delta$  is sufficiently small. Given failure probability  $\eta \in (0, 1)$ , if the parameters satisfy the following conditions:  $\tilde{I} \geq I$ ,*

$$T = \Omega\left(\frac{1}{\Delta} \log\left(\frac{KLR}{p_{\text{tail}}}\right)\right), \quad N = \Omega\left(\frac{LR}{p_{\text{tail}}^2} \log\left((J+K) \frac{LR}{\eta}\right)\right), \quad \sigma = \Omega\left(\log^{1/2}\left(\frac{\sqrt{LR}}{p_{\text{tail}}}\right)\right), \quad (\text{C1})$$

$$q = \mathcal{O}\left(\frac{p_{\text{tail}}}{(1+\sigma)\sqrt{KLR}}\right), \quad q = \mathcal{O}\left(\sqrt{\log\left(\frac{1+2\chi}{1+\chi}\right)}\right), \quad \alpha = \mathcal{O}(\Delta \cdot T), \quad (\text{C2})$$

and

$$T = \mathcal{O}\left(\frac{1}{\delta} \min\left\{\frac{p_{\text{tail}}}{(1+\sigma)\sqrt{KLR}}, \frac{p_{\text{tail}}^2}{KLR}\right\}\right), \quad \alpha = \Omega(\delta \cdot T), \quad (\text{C3})$$

$$C_p > 6(1+2\chi). \quad (\text{C4})$$

Here  $K = |\mathcal{D}|$ , and  $J = \left\lfloor \frac{2\pi T}{q} \right\rfloor$  is the number of candidate locations of cluster centers  $\{\theta_i\}$  in the block and searching algorithm.

Then, with probability at least  $1 - \eta$ , there exists a permutation  $\pi : [I] \rightarrow [I]$  such that the output of Algorithm 1  $\{(\theta_j^*, m_j)\}_{j \in [\tilde{I}]}$  satisfies the following guarantees:

$$\sup_{1 \leq j \leq I} |\theta_j^* - \lambda_{\pi(j)}^*| = \mathcal{O}\left((1+\sigma)\frac{p_{\text{tail}}}{p_{\text{min}}} \frac{1}{T}\right). \quad (\text{C5})$$

Furthermore, if  $p_{\text{tail}}/p_{\text{min}}, \delta$  are sufficiently small so that

$$\frac{1 - \mathcal{O}\left(((1+\sigma)p_{\text{tail}}/p_{\text{min}} + \delta \cdot T)^2\right)}{(1+\chi)^2} = \Omega\left(\frac{p_{\text{tail}}}{p_{\text{min}}}\right). \quad (\text{C6})$$

we can choose  $\tau = \Theta(p_{\text{tail}})$ , and  $\alpha = \Omega(\log(KLR/p_{\text{tail}}))$  to ensure that, with probability at least  $1 - \eta$ , we have

$$m_j = |\mathcal{D}_{\pi(j)}|, \quad 1 \leq j \leq I, \quad m_j = 0, \quad j > I. \quad (\text{C7})$$

*Remark C.3.* Here, we give some comments about the conditions and assumptions in the above theorem:

- The conditions Eq. (C1) and Eq. (C2) are similar to those in [23, Theorem 3.2], which ensure the algorithm can identify each cluster separately.
- In the above theorem, Eq. (C3) essentially requires that  $\delta$  is sufficiently small so that all dominant eigenvalues within a cluster can be approximated by a single output. When  $T = \Theta(\alpha/\delta)$ , the analysis becomes more involved, as a single cluster may yield multiple outputs, making the second step of the algorithm difficult to track.
- Eq. (C4) can be referred to as the sufficient domination condition, where  $C_p$  defines the set of dominant eigenstates in Theorem III.1.
- Although the condition Eq. (C6) appears technical, it essentially requires that  $\chi$  and  $p_{\text{tail}}$  are small so that the right-hand side is close to 1. This condition ensures a separation between the singular values of  $\mathcal{W}_j$ , which is necessary for accurately counting the number of dominant eigenvalues in each cluster.

*Remark C.4.* Together, the outputs of the location and multiplicity estimation define an approximate density  $\tilde{\mu}$  which approximates the true density  $\mu_D$  up to a small error in Wasserstein distance. Let  $\theta_i^*$  be the estimated center of  $\mathcal{I}_i$ . Define

$$\begin{aligned} \tilde{\mu}(E) &:= \frac{1}{|\mathcal{D}|} \sum_{i \in I} m_i \delta(E - \theta_i^*), \\ \mu_D(E) &:= \frac{1}{|\mathcal{D}|} \sum_{i \in \mathcal{D}} \delta(E - \lambda_i). \end{aligned} \quad (\text{C8})$$

Consider a transport map that transports each atom at  $E_j$  in  $\mathcal{I}_i$  to  $\theta_i^*$ . The cost is

$$|E_j - \theta_i^*| \leq |E_j - \lambda_i^*| + |\lambda_i^* - \theta_i^*| \leq \epsilon + \frac{\delta}{2}. \quad (\text{C9})$$

Averaging over the  $D$  atoms gives that

$$W_1(\mu_D, \tilde{\mu}) \leq \epsilon + \frac{\delta}{2}. \quad (\text{C10})$$

*Proof.* The proof strategy of [Theorem C.2](#) is similar to the proof of [23, Theorem 3.2]. We first show a rough estimation for the location of the clusters and then refine it to get a more accurate estimation. First of all, let us define the exact filter matrix  $\mathcal{F}(\theta)$ , the data matrix  $G(\theta)$  that approximates  $\mathcal{F}(\theta)$ , the error matrix  $E(\theta)$ , and the computed filter value function  $\mathcal{W}(\theta)$ :

$$\begin{aligned} \mathcal{F}(\theta) &:= \Phi \cdot \text{diag}(\{\exp(-(\theta - \lambda_m)^2 T^2)\}_{m \in [M]}) \cdot \Psi^\dagger \in \mathbb{C}^{L \times R}, \\ G(\theta) &:= \frac{1}{N} \sum_{n=1}^N Z_n \exp(i\theta t_n) \in \mathbb{C}^{L \times R}, \\ \mathcal{E}(\theta) &:= G(\theta) - \mathcal{F}(\theta) \in \mathbb{C}^{L \times R}, \\ \mathcal{W}(\theta) &:= \|G(\theta)\|_F \in \mathbb{R}. \end{aligned} \quad (\text{C11})$$

**Step 0:** We show that the computed filter value function  $\mathcal{W}(\theta)$  well approximates  $\|\mathcal{F}(\theta)\|_F$ .

Since  $\sigma = \Omega\left(\log^{1/2}\left(\frac{\sqrt{LR}}{p_{\text{tail}}}\right)\right)$  and  $N = \Omega\left(\frac{LR}{p_{\text{tail}}^2} \log\left((J+K)\frac{LR}{\eta}\right)\right)$ , according to [Theorem C.5](#) with  $\beta = p_{\text{tail}}/8$ , we have

$$\sup_{\theta_j} |\mathcal{W}(\theta_j) - \|\mathcal{F}(\theta_j)\|_F| \leq \sup_{\theta_j} \|\mathcal{E}(\theta_j)\|_F \leq \frac{p_{\text{tail}}}{8} \quad (\text{C12})$$

with probability at least  $1 - \eta/2$ . For simplicity, we only consider the case when [Eq. \(C12\)](#) is satisfied, which is true with probability at least  $1 - \eta/2$ .

**Step 1:** For each  $\theta_j^*$ , let  $\pi_j = \arg \min_i \{\text{dist}(\theta_j^*, I_i)\}$ . We show

$$\sup_{1 \leq j \leq I} |\theta_j^* - \lambda_{\pi_j}^*| = \sqrt{\log\left(\frac{2(1+2\chi)}{1+\chi}\right)} \frac{1}{T} \quad (\text{C13})$$

when [Eq. \(C12\)](#) holds true. To achieve this, we need to prove lower and upper bounds for  $\mathcal{W}(\theta)$ :

- If  $\theta \in (\cup_i [\lambda_i^* - \frac{q}{2T}, \lambda_i^* + \frac{q}{2T}]) \cap \{\theta_j\}_{j=1}^J$ , there exists  $\pi_\theta$  (index of the cluster that  $\theta$  belongs to) such that

$$\begin{aligned} \max_m \{|\theta - \lambda_m| : m \in \mathcal{D}_{\pi_\theta}\} &\leq \frac{q}{2T} + \frac{\delta}{2}, \\ \min_m \{|\theta - \lambda_m| : m \in \mathcal{D} \setminus \mathcal{D}_{\pi_\theta}\} &\geq \Delta - \frac{q}{2T} \geq \Delta/2, \end{aligned} \quad (\text{C14})$$

where we use  $T \geq \frac{q}{\Delta}$  to ensure the second inequality holds. This implies that  $\theta$  lies within a single cluster and is at least a distance of  $\Delta/2$  from any other cluster.

Using [Eq. \(C12\)](#) and the triangle inequality for the Frobenius norm, we observe that

$$\begin{aligned} \mathcal{W}(\theta) &\geq \left\| \Phi_{:, \mathcal{D}_{\pi_\theta}} \cdot \text{diag}(\{\exp(-(\theta - \lambda_m)^2 T^2)\}_{m \in \mathcal{D}_{\pi_\theta}}) \cdot (\Psi_{:, \mathcal{D}_{\pi_\theta}})^\dagger \right\|_F \\ &\quad - \sum_{i \neq \pi_\theta} \left\| \Phi_{:, \mathcal{D}_i} \cdot \text{diag}(\{\exp(-(\theta - \lambda_m)^2 T^2)\}_{m \in \mathcal{D}_i}) \cdot (\Psi_{:, \mathcal{D}_i})^\dagger \right\|_F \\ &\quad - \left\| \Phi_{:, \mathcal{D}^c} \cdot \text{diag}(\{\exp(-(\theta - \lambda_m)^2 T^2)\}_{m \in \mathcal{D}^c}) \cdot (\Psi_{:, \mathcal{D}^c})^\dagger \right\|_F - \frac{p_{\text{tail}}}{8} \end{aligned} \quad (\text{C15})$$

For the second term, using the second inequality of [Eq. \(C14\)](#) and [Theorem C.6 Eq. \(C64\)](#), we have

$$\begin{aligned}
& \sum_{i \neq \pi_\theta} \left\| \Phi_{:, \mathcal{D}_i} \cdot \text{diag} \left( \{ \exp(-(\theta - \lambda_m)^2 T^2) \}_{m \in \mathcal{D}_i} \right) \cdot (\Psi_{:, \mathcal{D}_i})^\dagger \right\|_F \\
& \leq \exp(-\Delta^2 T^2 / 4) \sum_{i \neq \pi_\theta} \sum_{m \in \mathcal{D}_i} \sqrt{\left( \sum_{l=1}^L |\Phi_{l,m}|^2 \right) \left( \sum_{r=1}^R |\Psi_{r,m}|^2 \right)} \\
& \leq \exp(-\Delta^2 T^2 / 4) \sqrt{K-1} \sqrt{\sum_{i \neq \pi_\theta} \sum_{m \in \mathcal{D}_i} \left( \sum_{l=1}^L |\Phi_{l,m}|^2 \right) \left( \sum_{r=1}^R |\Psi_{r,m}|^2 \right)} \\
& \leq \exp(-\Delta^2 T^2 / 4) \sqrt{K-1} \sqrt{\sum_{i \neq \pi_\theta} \sum_{m \in \mathcal{D}_i} \sum_{l=1}^L |\Phi_{l,m}|^2 R} \\
& \leq \sqrt{KLR} \exp(-\Delta^2 T^2 / 4) \leq \frac{p_{\text{tail}}}{8}.
\end{aligned} \tag{C16}$$

where we use Hölder's inequality in the second inequality and  $T = \Omega(\frac{1}{\Delta} \log(KLR/p_{\text{tail}}))$  in the last inequality. Similarly, for the third term, we have

$$\begin{aligned}
& \left\| \Phi_{:, \mathcal{D}^c} \cdot \text{diag} \left( \{ \exp(-(\theta - \lambda_m)^2 T^2) \}_{m \in \mathcal{D}^c} \right) \cdot (\Psi_{:, \mathcal{D}^c})^\dagger \right\|_F \\
& \leq \sum_{m \in \mathcal{D}^c} \sqrt{\left( \sum_{l=1}^L |\Phi_{l,m}|^2 \right) \left( \sum_{r=1}^R |\Psi_{r,m}|^2 \right)} = p_{\text{tail}}.
\end{aligned} \tag{C17}$$

Plugging these two inequalities into [Eq. \(C15\)](#), we have

$$\mathcal{W}(\theta) \geq \left\| \Phi_{:, \mathcal{D}_{\pi_\theta}} \cdot \text{diag} \left( \{ \exp(-(\theta - \lambda_m)^2 T^2) \}_{m \in \mathcal{D}_{\pi_\theta}} \right) \cdot (\Psi_{:, \mathcal{D}_{\pi_\theta}})^\dagger \right\|_F - \frac{5}{4} p_{\text{tail}}. \tag{C18}$$

For the first term, we notice that  $|\lambda_m - \lambda_{\pi_\theta}^*| \leq \delta$  when  $m \in \mathcal{D}_{\pi_\theta}$ . Combining this and [Theorem C.6 Eq. \(C64\)](#) we have

$$\begin{aligned}
& \left\| \Phi_{:, \mathcal{D}_{\pi_\theta}} \cdot \text{diag} \left( \{ \exp(-(\theta - \lambda_m)^2 T^2) - \exp(-(\theta - \lambda_{\pi_\theta}^*)^2 T^2) \}_{m \in \mathcal{D}_{\pi_\theta}} \right) \cdot (\Psi_{:, \mathcal{D}_{\pi_\theta}})^\dagger \right\|_F \\
& \leq \delta \cdot T \sum_{m \in [\mathcal{D}_{\pi_\theta}]} \sqrt{\left( \sum_{l=1}^L |\Phi_{l,m}|^2 \right) \left( \sum_{r=1}^R |\Psi_{r,m}|^2 \right)} \leq \delta \cdot T \sqrt{KLR} \leq \frac{p_{\text{tail}}}{4},
\end{aligned} \tag{C19}$$

where we use  $\delta = \mathcal{O}(p_{\text{tail}}/(\sqrt{KLR}T))$  in the last equality. This gives

$$\begin{aligned}
& \left\| \Phi_{:, \mathcal{D}_{\pi_\theta}} \cdot \text{diag} \left( \{ \exp(-(\theta - \lambda_m)^2 T^2) \}_{m \in \mathcal{D}_{\pi_\theta}} \right) \cdot (\Psi_{:, \mathcal{D}_{\pi_\theta}})^\dagger \right\|_F \\
& \geq \left\| \Phi_{:, \mathcal{D}_{\pi_\theta}} \cdot \underbrace{\text{diag} \left( \{ \exp(-(\theta - \lambda_{\pi_\theta}^*)^2 T^2) \}_{m \in \mathcal{D}_{\pi_\theta}} \right)}_{\text{constant diagonal}} \cdot (\Psi_{:, \mathcal{D}_{\pi_\theta}})^\dagger \right\|_F - \frac{p_{\text{tail}}}{4} \\
& \geq \exp \left( - \left( \frac{q}{2T} \right)^2 T^2 \right) \left\| \Phi_{:, \mathcal{D}_{\pi_\theta}} (\Psi_{:, \mathcal{D}_{\pi_\theta}})^\dagger \right\|_F - \frac{p_{\text{tail}}}{4} \\
& \geq \frac{1+\chi}{1+2\chi} \left\| \Phi_{:, \mathcal{D}_{\pi_\theta}} (\Psi_{:, \mathcal{D}_{\pi_\theta}})^\dagger \right\|_F - \frac{p_{\text{tail}}}{4}
\end{aligned} \tag{C20}$$

where we use the fact  $q = \mathcal{O} \left( \sqrt{\log \left( \frac{1+2\chi}{1+\chi} \right)} \right)$  in the last inequality.

Finally, plugging this into [Eq. \(C18\)](#), we obtain that

$$\mathcal{W}(\theta) \geq \frac{1+\chi}{1+2\chi} \left\| \Phi_{:, \mathcal{D}_{\pi_\theta}} \left( \Psi_{:, \mathcal{D}_{\pi_\theta}} \right)^\dagger \right\|_F - \frac{3}{2} p_{\text{tail}}. \quad (\text{C21})$$

This gives an lower bound of  $\mathcal{W}(\theta)$  if  $\theta \in (\cup_i [\lambda_i^* - \frac{q}{2T}, \lambda_i^* + \frac{q}{2T}]) \cap \{\theta_j\}_{j=1}^J$ .

- Similar to the above calculation and using [Eq. \(C12\)](#), [Eq. \(C19\)](#) and [Theorem C.6](#) [Eq. \(C64\)](#) for the first term, we have

$$\begin{aligned} \mathcal{W}(\theta_j^*) &\leq \left\| \Phi_{:, \mathcal{D}_{\pi_j}} \cdot \text{diag} \left( \left\{ \exp(-(\theta_j^* - \lambda_m)^2 T^2) \right\}_{m \in \mathcal{D}_{\pi_j}} \right) \cdot \left( \Psi_{:, \mathcal{D}_{\pi_j}} \right)^\dagger \right\|_F \\ &\quad + \underbrace{\sum_{i \neq \pi_j} \left\| \Phi_{:, \mathcal{D}_i} \cdot \text{diag} \left( \left\{ \exp(-(\theta_j^* - \lambda_m)^2 T^2) \right\}_{m \in \mathcal{D}_i} \right) \cdot \left( \Psi_{:, \mathcal{D}_i} \right)^\dagger \right\|_F}_{\leq \sqrt{KLR} \exp(-\Delta^2 T^2/4) \leq \frac{p_{\text{tail}}}{8}} \\ &\quad + \underbrace{\left\| \Phi_{:, \mathcal{D}^c} \cdot \text{diag} \left( \left\{ \exp(-(\theta_j^* - \lambda_m)^2 T^2) \right\}_{m \in \mathcal{D}^c} \right) \cdot \left( \Psi_{:, \mathcal{D}^c} \right)^\dagger \right\|_F + \frac{p_{\text{tail}}}{8}}_{\leq p_{\text{tail}}} \\ &\leq \left\| \Phi_{:, \mathcal{D}_{\pi_j}} \cdot \text{diag} \left( \left\{ \exp(-(\theta_j^* - \lambda_m)^2 T^2) \right\}_{m \in \mathcal{D}_{\pi_j}} \right) \cdot \left( \Psi_{:, \mathcal{D}_{\pi_j}} \right)^\dagger \right\|_F + \frac{5}{4} p_{\text{tail}} \\ &\leq \exp(-(\theta_j^* - \lambda_{\pi_j}^*)^2 T^2) \left\| \Phi_{:, \mathcal{D}_{\pi_j}} \left( \Psi_{:, \mathcal{D}_{\pi_j}} \right)^\dagger \right\|_F + \frac{3}{2} p_{\text{tail}}. \end{aligned} \quad (\text{C22})$$

This gives an upper bound of  $\mathcal{W}(\theta_j^*)$ .

According to [Eqs. \(C21\)](#) and [\(C22\)](#), when  $j = 1$ , because  $\mathcal{W}(\theta_1^*)$  takes the maximal value, we have

$$\exp(-(\theta_1^* - \lambda_{\pi_1}^*)^2 T^2) \left\| \Phi_{:, \mathcal{D}_{\pi_1}} \left( \Psi_{:, \mathcal{D}_{\pi_1}} \right)^\dagger \right\|_F + \frac{3}{2} p_{\text{tail}} \geq \mathcal{W}(\theta_1^*) \geq \frac{1+\chi}{1+2\chi} \left\| \Phi_{:, \mathcal{D}_{\pi_1}} \left( \Psi_{:, \mathcal{D}_{\pi_1}} \right)^\dagger \right\|_F - \frac{3}{2} p_{\text{tail}}, \quad (\text{C23})$$

where the second inequality holds since there must exist some grid point  $\theta_1$  such that  $\theta_1 \in [\lambda_{\pi_1}^* - \frac{q}{2T}, \lambda_{\pi_1}^* + \frac{q}{2T}]$  and  $\mathcal{W}(\theta_1^*) \geq \mathcal{W}(\theta_1)$  by definition. Thus,

$$\begin{aligned} \exp(-(\theta_1^* - \lambda_{\pi_1}^*)^2 T^2) \left\| \Phi_{:, \mathcal{D}_{\pi_1}} \left( \Psi_{:, \mathcal{D}_{\pi_1}} \right)^\dagger \right\|_F + \frac{3}{2} p_{\text{tail}} &\geq \frac{1+\chi}{1+2\chi} \left\| \Phi_{:, \mathcal{D}_{\pi_1}} \left( \Psi_{:, \mathcal{D}_{\pi_1}} \right)^\dagger \right\|_F - \frac{3}{2} p_{\text{tail}} \\ \implies |\theta_1^* - \lambda_{\pi_1}^*| &\leq \log^{1/2} \left( \frac{1}{\frac{1+\chi}{2+\chi} - 3p_{\text{tail}}/\left\| \Phi_{:, \mathcal{D}_{\pi_1}} \left( \Psi_{:, \mathcal{D}_{\pi_1}} \right)^\dagger \right\|_F} \right) \frac{1}{T} \end{aligned} \quad (\text{C24})$$

We further note that,

$$\begin{aligned}
\left\| \Phi_{:, \mathcal{D}_{\pi_\theta}} \left( \Psi_{:, \mathcal{D}_{\pi_\theta}} \right)^\dagger \right\|_F^2 &= \text{Tr} \left( \Psi_{:, \mathcal{D}_{\pi_\theta}} \left( \Phi_{:, \mathcal{D}_{\pi_\theta}} \right)^\dagger \Phi_{:, \mathcal{D}_{\pi_\theta}} \left( \Psi_{:, \mathcal{D}_{\pi_\theta}} \right)^\dagger \right) \\
&\geq \lambda_{\min} \left( \left( \Phi_{:, \mathcal{D}_{\pi_\theta}} \right)^\dagger \Phi_{:, \mathcal{D}_{\pi_\theta}} \right) \text{Tr} \left( \left( \Psi_{:, \mathcal{D}_{\pi_\theta}} \right)^\dagger \Psi_{:, \mathcal{D}_{\pi_\theta}} \right) \\
&= \lambda_{\min} \left( \left( \Phi_{:, \mathcal{D}_{\pi_\theta}} \right)^\dagger \Phi_{:, \mathcal{D}_{\pi_\theta}} \right) \left( \sum_{i \in \mathcal{D}_{\pi_\theta}} \sum_{k=1}^R |\Psi_{k,i}|^2 \right) \\
&\geq \left( \frac{1}{1+\chi} \right)^2 \frac{1}{|\mathcal{D}_{\pi_\theta}|} \text{Tr} \left( \left( \Phi_{:, \mathcal{D}_{\pi_\theta}} \right)^\dagger \Phi_{:, \mathcal{D}_{\pi_\theta}} \right) \left( \sum_{i \in \mathcal{D}_{\pi_\theta}} \sum_{k=1}^R |\Psi_{k,i}|^2 \right) \\
&= \left( \frac{1}{1+\chi} \right)^2 \frac{1}{|\mathcal{D}_{\pi_\theta}|} \left( \sum_{j \in \mathcal{D}_{\pi_\theta}} \sum_{k=1}^L |\Phi_{k,j}|^2 \right) \left( \sum_{i \in \mathcal{D}_{\pi_\theta}} \sum_{k=1}^R |\Psi_{k,i}|^2 \right) \\
&\geq \left( \frac{1}{1+\chi} \right)^2 \frac{1}{|\mathcal{D}_{\pi_\theta}|} \left( \sum_{i \in \mathcal{D}_{\pi_\theta}} \left( \sum_{k=1}^L |\Phi_{k,i}|^2 \right) \left( \sum_{k=1}^R |\Psi_{k,i}|^2 \right) \right) \\
&\geq \left( \frac{1}{1+\chi} \right)^2 p_{\min}^2.
\end{aligned} \tag{C25}$$

The second inequality comes from [Assumption 1](#). Plugging this bound into the above inequality, we have

$$|\theta_1^* - \lambda_{\pi_1}^*| < \sqrt{\log \left( \frac{1}{\frac{1+\chi}{2+\chi} - 3(1+\chi)p_{\text{tail}}/p_{\min}} \right) \frac{1}{T}} \leq \sqrt{\log \left( \frac{2(1+2\chi)}{1+\chi} \right) \frac{1}{T}}. \tag{C26}$$

where we use  $3p_{\text{tail}}/p_{\min} \leq \frac{1}{2(1+2\chi)}$  ([Eq. \(C4\)](#)) in the last step.

Furthermore, since  $\text{dist}(I_i, I_j) > \Delta$ ,  $T = \Omega((1+\alpha+q)/\Delta)$  and  $\delta \ll \Delta$ , we have

$$\left[ \theta_1^* - \frac{\alpha}{T}, \theta_1^* + \frac{\alpha}{T} \right] \cap \left( \cup_{i \neq \pi_1} \left[ \lambda_i^* - \frac{q}{2T}, \lambda_i^* + \frac{q}{2T} \right] \right) = \emptyset \tag{C27}$$

This implies that the first block interval does not overlap with  $\cup_{i \neq \pi_1} \left[ \lambda_i^* - \frac{q}{2T}, \lambda_i^* + \frac{q}{2T} \right]$ . In addition,  $\alpha = \Omega \left( \max \left\{ \sqrt{\log \left( \frac{2(1+2\chi)}{1+\chi} \right)}, \delta \cdot T \right\} \right)$ , we have  $i_2 \neq \pi_1$ , meaning  $\theta_2^*$  is not close to  $\lambda_{\pi_1}^*$ . More specifically, by [Eq. \(C27\)](#), we can repeat the above argument for  $\theta_2^*$  and obtain

$$|\theta_2^* - \lambda_{i_2}^*| \leq \sqrt{\log \left( \frac{2(1+2\chi)}{1+\chi} \right) \frac{1}{T}} = \mathcal{O} \left( \frac{\alpha}{T} \right). \tag{C28}$$

If  $i_2 = \pi_1$ , then by [Eq. \(C26\)](#) and triangle inequality, we have

$$|\theta_2^* - \theta_1^*| \leq |\theta_2^* - \lambda_{\pi_1}^*| + |\theta_1^* - \lambda_{\pi_1}^*| < \frac{\alpha}{T}, \tag{C29}$$

which is impossible since the grid points that are  $\frac{\alpha}{T}$ -close to  $\theta_1^*$  have been blocked.

Repeating this argument for all  $1 \leq j \leq I$ , we can show

$$|\theta_j^* - \lambda_{\pi_j}^*| \leq \sqrt{\log \left( \frac{2(1+2\chi)}{1+\chi} \right) \frac{1}{T}} \tag{C30}$$

for all  $1 \leq j \leq I$ .

**Step 2:** Using the result obtained in Step 1, we can impose stronger bounds on  $\mathcal{W}(\theta)$  to refine the error estimation. We will show

$$\sup_{1 \leq j \leq I} |\theta_j^* - \lambda_{\pi_j}^*| = \mathcal{O} \left( (1+\sigma) \frac{p_{\text{tail}}}{p_{\min}} \frac{1}{T} \right) \tag{C31}$$

when [Eq. \(C12\)](#) holds true.

Without loss of generality, we only consider  $j = 1$ . The other cases can be improved similarly. Let us pick  $\tilde{\theta}_1^* \in [\lambda_{\pi_1}^* - \frac{q}{2T}, \lambda_{\pi_1}^* + \frac{q}{2T}] \cap \{\theta_j\}_{j=1}^J$ , which is the closest energy grid point to the desired cluster center  $\lambda_{\pi_1}^*$ . It can vary from our computed estimate  $\theta_1^*$  due to the errors arising from noise, contributions of non-dominant eigenvectors, and of dominant eigenvectors in distant clusters, and it holds that  $\mathcal{W}(\theta_1^*) \geq \mathcal{W}(\tilde{\theta}_1^*)$ . We will bound the distance between  $\theta_1^*$  and  $\tilde{\theta}_1^*$ , and thus between  $\theta_1^*$  and  $\lambda_{\pi_1}^*$ .

We first define

$$\begin{aligned} G(\theta) = & \underbrace{\Phi_{:, \mathcal{D}_{\pi_1}} \cdot \text{diag} \left( \left\{ \exp(-(\theta - \lambda_m)^2 T^2) \right\}_{m \in \mathcal{D}_{\pi_1}} \right) \cdot (\Psi_{:, \mathcal{D}_{\pi_1}})^\dagger}_{:=A(\theta)} \\ & + \underbrace{\Phi_{:, \mathcal{D}^c} \cdot \text{diag} \left( \left\{ \exp(-(\theta - \lambda_m)^2 T^2) \right\}_{m \in \mathcal{D}^c} \right) \cdot (\Psi_{:, \mathcal{D}^c})^\dagger}_{:=B(\theta)} \\ & + \underbrace{\sum_{i \neq \pi_1} \Phi_{:, \mathcal{D}_i} \cdot \text{diag} \left( \left\{ \exp(-(\theta - \lambda_m)^2 T^2) \right\}_{m \in \mathcal{D}_i} \right) \cdot (\Psi_{:, \mathcal{D}_i})^\dagger + \mathcal{E}(\theta)}_{:=C(\theta)}. \end{aligned} \quad (\text{C32})$$

According to [Eq. \(C22\)](#), [Eq. \(C12\)](#) and [Eq. \(C16\)](#), we have

$$\begin{aligned} \|A(\theta_1^*)\|_F & \leq \exp(-(\theta_1^* - \lambda_{\pi_1})^2 T^2) \left\| \Phi_{:, \mathcal{D}_{\pi_1}} (\Psi_{:, \mathcal{D}_{\pi_1}})^\dagger \right\|_F + \frac{1}{4} p_{\text{tail}} \leq \frac{5}{4} \left\| \Phi_{:, \mathcal{D}_{\pi_1}} (\Psi_{:, \mathcal{D}_{\pi_1}})^\dagger \right\|_F, \\ \|A(\tilde{\theta}_1^*)\|_F & \leq \exp\left(-\left(\tilde{\theta}_1^* - \lambda_{\pi_1}\right)^2 T^2\right) \left\| \Phi_{:, \mathcal{D}_{\pi_1}} (\Psi_{:, \mathcal{D}_{\pi_1}})^\dagger \right\|_F + \frac{1}{4} p_{\text{tail}} \leq \frac{5}{4} \left\| \Phi_{:, \mathcal{D}_{\pi_1}} (\Psi_{:, \mathcal{D}_{\pi_1}})^\dagger \right\|_F, \end{aligned} \quad (\text{C33})$$

where we use  $p_{\text{tail}} < \frac{p_{\min}}{1+\chi} \leq \left\| \Phi_{:, \mathcal{D}_{\pi_1}} (\Psi_{:, \mathcal{D}_{\pi_1}})^\dagger \right\|_F$  according to [Eq. \(C25\)](#) in the second inequalities, and

$$\|B(\theta_1^*) + C(\theta_1^*) + \mathcal{E}(\theta_1^*)\|_F \leq \frac{5p_{\text{tail}}}{4}, \quad \|B(\tilde{\theta}_1^*) + C(\tilde{\theta}_1^*) + \mathcal{E}(\tilde{\theta}_1^*)\|_F \leq \frac{5p_{\text{tail}}}{4}. \quad (\text{C34})$$

Then, we get that

$$\begin{aligned} \mathcal{W}^2(\theta) & = \text{Tr}(G^\dagger(\theta)G(\theta)) \\ & = \text{Tr}(A^\dagger(\theta)A(\theta)) + 2\text{Re}(\text{Tr}(A^\dagger(\theta)(B(\theta) + C(\theta) + \mathcal{E}(\theta)))) \\ & \quad + \text{Tr}((B^\dagger(\theta) + C^\dagger(\theta) + \mathcal{E}^\dagger(\theta))(B(\theta) + C(\theta) + \mathcal{E}(\theta))). \end{aligned} \quad (\text{C35})$$

We first deal with the first term, the last term, and then the second term:

- For the first term, we have

$$\begin{aligned} A(\theta) = & \Phi_{:, \mathcal{D}_{\pi_1}} \cdot \text{diag} \left( \left\{ \exp(-(\theta - \lambda_{\pi_1}^*)^2 T^2) \right\}_{m \in \mathcal{D}_{\pi_1}} \right) \cdot (\Psi_{:, \mathcal{D}_{\pi_1}})^\dagger \\ & + \Phi_{:, \mathcal{D}_{\pi_1}} \cdot \text{diag} \left( \left\{ \exp(-(\theta - \lambda_m)^2 T^2) - \exp(-(\theta - \lambda_{\pi_1}^*)^2 T^2) \right\}_{m \in \mathcal{D}_{\pi_1}} \right) \cdot (\Psi_{:, \mathcal{D}_{\pi_1}})^\dagger. \end{aligned} \quad (\text{C36})$$

Noticing  $|\lambda_m - \lambda_{\pi_1}^*| \leq \delta$  when  $m \in \mathcal{D}_{\pi_1}$ , we have

$$\left\| \Phi_{:, \mathcal{D}_{\pi_1}} \cdot \text{diag} \left( \left\{ \exp(-(\theta - \lambda_m)^2 T^2) - \exp(-(\theta - \lambda_{\pi_1}^*)^2 T^2) \right\}_{m \in \mathcal{D}_{\pi_1}} \right) \cdot (\Psi_{:, \mathcal{D}_{\pi_1}})^\dagger \right\|_F \leq \sqrt{KLR} \delta \cdot T \quad (\text{C37})$$

according to [Theorem C.6](#) [Eq. \(C65\)](#). Thus, we obtain that

$$\left| \|A(\theta)\|_F - \left\| \Phi_{:, \mathcal{D}_{\pi_1}} \cdot \text{diag} \left( \left\{ \exp(-(\theta - \lambda_{\pi_1}^*)^2 T^2) \right\}_{m \in \mathcal{D}_{\pi_1}} \right) \cdot (\Psi_{:, \mathcal{D}_{\pi_1}})^\dagger \right\|_F \right| \leq \sqrt{KLR} \delta \cdot T, \quad (\text{C38})$$

where we use  $\delta \cdot T < 1$ .

- For the last term, by [Eq. \(C34\)](#), we have

$$\begin{aligned} \text{Tr}((B^\dagger(\theta_1^*) + C^\dagger(\theta_1^*) + \mathcal{E}^\dagger(\theta_1^*))(B(\theta_1^*) + C(\theta_1^*) + \mathcal{E}(\theta_1^*))) & \leq \frac{9}{4} p_{\text{tail}}^2, \\ \text{Tr}((B^\dagger(\tilde{\theta}_1^*) + C^\dagger(\tilde{\theta}_1^*) + \mathcal{E}^\dagger(\tilde{\theta}_1^*))(B(\tilde{\theta}_1^*) + C(\tilde{\theta}_1^*) + \mathcal{E}(\tilde{\theta}_1^*))) & \leq \frac{9}{4} p_{\text{tail}}^2. \end{aligned} \quad (\text{C39})$$

- For the second term, we have

$$\begin{aligned}
& 2\operatorname{Re}(\operatorname{Tr}(A^\dagger(\theta_1^*)(B(\theta_1^*) + C(\theta_1^*) + \mathcal{E}(\theta_1^*))) - 2\operatorname{Re}(\operatorname{Tr}(A^\dagger(\tilde{\theta}_1^*)(B(\tilde{\theta}_1^*) + C(\tilde{\theta}_1^*) + \mathcal{E}(\tilde{\theta}_1^*)))) \\
& \leq 2 \left\| A(\theta_1^*) - A(\tilde{\theta}_1^*) \right\|_F \left\| (B(\theta_1^*) + C(\theta_1^*) + \mathcal{E}(\theta_1^*)) \right\|_F \\
& \quad + 2 \left\| A(\tilde{\theta}_1^*) \right\|_F \left\| (B(\theta_1^*) + C(\theta_1^*) + \mathcal{E}(\theta_1^*)) - (B(\tilde{\theta}_1^*) + C(\tilde{\theta}_1^*) + \mathcal{E}(\tilde{\theta}_1^*)) \right\|_F.
\end{aligned} \tag{C40}$$

Similar to the calculation in [Eq. \(C19\)](#), we obtain from [Eq. \(C38\)](#) that

$$\begin{aligned}
\left\| A(\theta_1^*) - A(\tilde{\theta}_1^*) \right\|_F & \leq T \left| \theta_1^* - \tilde{\theta}_1^* \right| \left\| \Phi_{:, \mathcal{D}_{\pi_1}} (\Psi_{:, \mathcal{D}_{\pi_1}})^\dagger \right\|_F + 2\sqrt{KLR}\delta \cdot T \\
& \leq T \left| \theta_1^* - \tilde{\theta}_1^* \right| \left\| \Phi_{:, \mathcal{D}_{\pi_1}} (\Psi_{:, \mathcal{D}_{\pi_1}})^\dagger \right\|_F + \frac{p_{\text{tail}}}{2},
\end{aligned} \tag{C41}$$

where we use  $\delta \cdot T = \mathcal{O}(p_{\text{tail}}/\sqrt{KLR})$  in the last inequality. According to [Theorem C.6](#) [Eq. \(C65\)](#) and [Theorem C.5](#) [Eq. \(C58\)](#), we have

$$\|B(\theta) - B(\theta')\|_F \leq p_{\text{tail}}\sigma T|\theta - \theta'|/2, \quad \Pr[\forall \theta \neq \theta' \in \Theta : \|\mathcal{E}(\theta) - \mathcal{E}(\theta')\|_F \leq p_{\text{tail}}\sigma T|\theta - \theta'|/2] \geq 1 - \frac{\eta}{2}. \tag{C42}$$

And we have

$$\begin{aligned}
& \|C(\theta) - C(\theta')\|_F \\
& \leq \sum_{i \neq \pi_1} \left\| \Phi_{:, \mathcal{D}_i} (\exp(-(\theta - \lambda_i^*)^2 T^2) - \exp(-(\theta' - \lambda_i^*)^2 T^2)) \Psi_{:, \mathcal{D}_i}^\dagger \right\|_F \\
& \quad + \sum_{i \neq \pi_1} \left\| \Phi_{:, \mathcal{D}_i} \operatorname{diag} \left( \{\exp(-(\theta - \lambda_m)^2 T^2) - \exp(-(\theta - \lambda_i^*)^2 T^2)\}_{m \in \mathcal{D}_i} \right) \Psi_{:, \mathcal{D}_i}^\dagger \right\|_F \\
& \quad + \sum_{i \neq \pi_1} \left\| \Phi_{:, \mathcal{D}_i} \operatorname{diag} \left( \{\exp(-(\theta' - \lambda_m)^2 T^2) - \exp(-(\theta' - \lambda_i^*)^2 T^2)\}_{m \in \mathcal{D}_i} \right) \Psi_{:, \mathcal{D}_i}^\dagger \right\|_F \\
& \leq \sum_{i \neq \pi_1} \left\| \Phi_{:, \mathcal{D}_i} (\exp(-(\theta - \lambda_i^*)^2 T^2) - \exp(-(\theta' - \lambda_i^*)^2 T^2)) \Psi_{:, \mathcal{D}_i}^\dagger \right\|_F \\
& \quad + 2\delta \cdot T\sqrt{KLR} \\
& \leq \sum_{i \neq \pi_1} \left| \exp(-(\theta - \lambda_i^*)^2 T^2) - \exp(-(\theta' - \lambda_i^*)^2 T^2) \right| \left\| \Phi_{:, \mathcal{D}_i} \Psi_{:, \mathcal{D}_i}^\dagger \right\|_F + \frac{p_{\text{tail}}^2}{4\sqrt{KLR}} \\
& \leq \frac{p_{\text{tail}}^2}{4\sqrt{KLR}} + o(p_{\text{tail}}T|\theta - \theta'|),
\end{aligned} \tag{C43}$$

where we use a similar calculation as [Eq. \(C19\)](#) and  $\delta \cdot T = \mathcal{O}(p_{\text{tail}}^2/KLR)$  in the second step. And the third step follows from

$$\begin{aligned}
(\exp(-(\theta - \lambda_i^*)^2 T^2) - \exp(-(\theta' - \lambda_i^*)^2 T^2)) & \leq T|\theta - \theta'| \left( \sup_{|x| \geq \min\{|\theta - \lambda_i^*|T, |\theta' - \lambda_i^*|T\}} 2x \exp(-x^2) \right) \\
& = o \left( \frac{p_{\text{tail}}T|\theta - \theta'|}{K\|\Phi_{:, \mathcal{D}_i} \Psi_{:, \mathcal{D}_i}^\dagger\|_F} \right),
\end{aligned}$$

where the last inequality comes from  $\min\{|\theta - \lambda_i^*|T, |\theta' - \lambda_i^*|T\} \geq \Delta^2 T^2/4$  and  $T = \Omega\left(\frac{1}{\Delta} \log\left(\frac{KLR}{p_{\text{tail}}}\right)\right)$ .

Plugging these three inequalities into the second term and using [Eq. \(C33\)](#) and [Eq. \(C34\)](#), we have probability

at least  $1 - \eta$  such that

$$\begin{aligned}
& 2\text{Re}(\text{Tr}(A^\dagger(\theta_1^*)(B(\theta_1^*) + C(\theta_1^*) + \mathcal{E}(\theta_1^*)))) - 2\text{Re}(\text{Tr}(A^\dagger(\tilde{\theta}_1^*)(B(\tilde{\theta}_1^*) + C(\tilde{\theta}_1^*) + \mathcal{E}(\tilde{\theta}_1^*)))) \\
& \leq 2 \left( T |\theta_1^* - \tilde{\theta}_1^*| \left\| \Phi_{:, \mathcal{D}_{\pi_1}} (\Psi_{:, \mathcal{D}_{\pi_1}})^\dagger \right\|_F + \frac{p_{\text{tail}}}{2} \right) \cdot \frac{5}{4} p_{\text{tail}} \\
& \quad + 2 \cdot \frac{5}{4} \left\| \Phi_{:, \mathcal{D}_{\pi_1}} (\Psi_{:, \mathcal{D}_{\pi_1}})^\dagger \right\|_F \cdot \left( 2p_{\text{tail}} \sigma T |\theta_1^* - \tilde{\theta}_1^*| + \frac{p_{\text{tail}}^2}{4\sqrt{KLR}} \right) \\
& \leq (3 + 5\sigma) \left\| \Phi_{:, \mathcal{D}_{\pi_1}} (\Psi_{:, \mathcal{D}_{\pi_1}})^\dagger \right\|_F T |\theta_1^* - \tilde{\theta}_1^*| p_{\text{tail}} + \frac{15}{8} p_{\text{tail}}^2 \\
& \leq (3 + 5\sigma) \left\| \Phi_{:, \mathcal{D}_{\pi_1}} (\Psi_{:, \mathcal{D}_{\pi_1}})^\dagger \right\|_F T \left( |\theta_1^* - \lambda_{\pi_1}^*| + \frac{q}{T} + \delta \right) p_{\text{tail}} + \frac{15}{8} p_{\text{tail}}^2 \\
& \leq (3 + 5\sigma) \left\| \Phi_{:, \mathcal{D}_{\pi_1}} (\Psi_{:, \mathcal{D}_{\pi_1}})^\dagger \right\|_F T |\theta_1^* - \lambda_{\pi_1}^*| p_{\text{tail}} + \frac{23}{8} p_{\text{tail}}^2,
\end{aligned} \tag{C44}$$

where we use  $\left\| \Phi_{:, \mathcal{D}_{\pi_1}} (\Psi_{:, \mathcal{D}_{\pi_1}})^\dagger \right\|_F \leq \sqrt{KLR}$  (according to similar calculation as [Eq. \(C16\)](#)) in the second inequality and  $q = \mathcal{O}(p_{\text{tail}}/((1 + \sigma)\sqrt{KLR}))$  and  $\delta = \mathcal{O}(p_{\text{tail}}/(T(1 + \sigma)\sqrt{KLR}))$  in the last inequality.

Now, plugging  $\theta = \theta_1^*$  and  $\theta = \tilde{\theta}_1^*$  into  $\mathcal{W}^2(\theta)$  and using [Eqs. \(C25\)](#) and [\(C38\)](#), we have

$$\begin{aligned}
0 & \leq \mathcal{W}^2(\theta_1^*) - \mathcal{W}^2(\tilde{\theta}_1^*) \\
& \leq \underbrace{\left( \exp\left(-2(\theta_1^* - \lambda_{\pi_1}^*)^2 T^2\right) - \exp\left(-2(\tilde{\theta}_1^* - \lambda_{\pi_1}^*)^2 T^2\right) \right)}_{\leq 0 \text{ by the definition of } \tilde{\theta}_1^*} \left\| \Phi_{:, \mathcal{D}_{\pi_1}} (\Psi_{:, \mathcal{D}_{\pi_1}})^\dagger \right\|_F^2 \\
& \quad + \underbrace{6KLR\delta \cdot T}_{\leq p_{\text{tail}}^2} + (3 + 5\sigma) \left\| \Phi_{:, \mathcal{D}_{\pi_1}} (\Psi_{:, \mathcal{D}_{\pi_1}})^\dagger \right\|_F T |\theta_1^* - \lambda_{\pi_1}^*| p_{\text{tail}} + \frac{23}{8} p_{\text{tail}}^2 + \underbrace{\frac{9}{2} p_{\text{tail}}^2}_{\text{last term}}.
\end{aligned} \tag{C45}$$

where we use the condition that  $\delta \cdot T = \mathcal{O}(p_{\text{tail}}^2/KLR)$ . Because we already show  $|\theta_1^* - \lambda_{\pi_1}^*| = \mathcal{O}(1/T)$  (noticing  $\chi = \mathcal{O}(1)$ ) in the first step, let  $\delta_\theta = T |\theta_1^* - \lambda_{\pi_1}^*|$ , the above inequality implies that

$$-C\delta_\theta^2 + \left( (3 + 5\sigma)p_{\text{tail}} / \left\| \Phi_{:, \mathcal{D}_{\pi_1}} (\Psi_{:, \mathcal{D}_{\pi_1}})^\dagger \right\|_F \right) \delta_\theta + \frac{67}{8} \frac{p_{\text{tail}}^2}{\left\| \Phi_{:, \mathcal{D}_{\pi_1}} (\Psi_{:, \mathcal{D}_{\pi_1}})^\dagger \right\|_F^2} \geq 0, \tag{C46}$$

where  $C$  is a uniform constant. Thus, we have that

$$|\theta_1^* - \lambda_{\pi_1}^*| = \mathcal{O}\left((1 + \sigma) \frac{p_{\text{tail}}}{\left\| \Phi_{:, \mathcal{D}_{\pi_1}} (\Psi_{:, \mathcal{D}_{\pi_1}})^\dagger \right\|_F} \frac{1}{T}\right) = \mathcal{O}\left((1 + \sigma) \frac{p_{\text{tail}}}{p_{\min}} \frac{1}{T}\right), \tag{C47}$$

where we use [Eq. \(C25\)](#) and  $\chi = \mathcal{O}(1)$  for the last equality. This concludes the first part of the proof.

**Step 3:** We show that  $m_{\pi_j} = |\mathcal{D}_{\pi_j}|$  when  $1 \leq j \leq I$ .

Without loss of generality, we only consider  $i = 1$ . The other cases can also be shown similarly. Define  $s_k(A)$  as the  $k$ -th singular value of  $A$ . Recall

$$\begin{aligned}
G(\theta_1^*) &= \underbrace{\Phi_{:, \mathcal{D}_{\pi_1}} \cdot \text{diag} \left( \left\{ \exp(-(\theta_1^* - \lambda_m)^2 T^2) \right\}_{m \in \mathcal{D}_{\pi_1}} \right) \cdot (\Psi_{:, \mathcal{D}_{\pi_1}})^\dagger}_{:= A(\theta_1^*)} \\
&\quad + \underbrace{\Phi_{:, \mathcal{D}^c} \cdot \text{diag} \left( \left\{ \exp(-(\theta_1^* - \lambda_m)^2 T^2) \right\}_{m \in \mathcal{D}^c} \right) \cdot (\Psi_{:, \mathcal{D}^c})^\dagger}_{:= B(\theta_1^*)} \\
&\quad + \underbrace{\sum_{i \neq \pi_1} \Phi_{:, \mathcal{D}_i} \cdot \text{diag} \left( \left\{ \exp(-(\theta_1^* - \lambda_m)^2 T^2) \right\}_{m \in \mathcal{D}_i} \right) \cdot (\Psi_{:, \mathcal{D}_i})^\dagger + \mathcal{E}(\theta_1^*)}_{:= C(\theta_1^*)}.
\end{aligned} \tag{C48}$$

With probability at least  $1 - \eta$ , we have

$$\|B(\theta_1^*) + C(\theta_1^*) + \mathcal{E}(\theta_1^*)\|_2 \leq \|B(\theta_1^*) + C(\theta_1^*) + \mathcal{E}(\theta_1^*)\|_F \leq 2p_{\text{tail}}. \quad (\text{C49})$$

Furthermore, for  $1 \leq k \leq |\mathcal{D}_{\pi_1}|$ , Eq. (C5) implies that

$$\begin{aligned} s_k(A(\theta_1^*)) &= \exp\left(-\mathcal{O}((1+\sigma)(p_{\text{tail}}/p_{\min}) + \delta \cdot T)^2\right) \left(\lambda_k\left(\Psi_{:, \mathcal{D}_{\pi_1}} \Phi_{:, \mathcal{D}_{\pi_1}}^\dagger \Phi_{:, \mathcal{D}_{\pi_1}} (\Psi_{:, \mathcal{D}_{\pi_1}})^\dagger\right)\right)^{1/2} \\ &\geq \exp\left(-\mathcal{O}((1+\sigma)(p_{\text{tail}}/p_{\min}) + \delta \cdot T)^2\right) \left(\lambda_{\min}(\Phi_{:, \mathcal{D}_{\pi_1}}^\dagger \Phi_{:, \mathcal{D}_{\pi_1}})\right)^{1/2} \left(\lambda_k(\Psi_{:, \mathcal{D}_{\pi_1}} (\Psi_{:, \mathcal{D}_{\pi_1}})^\dagger)\right)^{1/2} \\ &\geq \exp\left(-\mathcal{O}((1+\sigma)(p_{\text{tail}}/p_{\min}) + \delta \cdot T)^2\right) \left(\lambda_{\min}(\Phi_{:, \mathcal{D}_{\pi_1}}^\dagger \Phi_{:, \mathcal{D}_{\pi_1}})\right)^{1/2} \left(\lambda_{\min}(\Psi_{:, \mathcal{D}_{\pi_1}}^\dagger \Psi_{:, \mathcal{D}_{\pi_1}})\right)^{1/2} \\ &\geq \exp\left(-\mathcal{O}((1+\sigma)(p_{\text{tail}}/p_{\min}) + \delta \cdot T)^2\right) \left(\frac{1}{1+\chi}\right)^2 \frac{\|\Phi_{:, \mathcal{D}_i}\|_F \|\Psi_{:, \mathcal{D}_i}\|_F}{|\mathcal{D}_i|} \\ &= \exp\left(-\mathcal{O}((1+\sigma)(p_{\text{tail}}/p_{\min}) + \delta \cdot T)^2\right) \left(\frac{1}{1+\chi}\right)^2 \frac{\sqrt{\sum_{m \in \mathcal{D}_i} \|\Phi_{:, m}\|^2} \sqrt{\sum_{m \in \mathcal{D}_i} \|\Psi_{:, m}\|^2}}{|\mathcal{D}_i|} \\ &\geq \exp\left(-\mathcal{O}((1+\sigma)(p_{\text{tail}}/p_{\min}) + \delta \cdot T)^2\right) \left(\frac{1}{1+\chi}\right)^2 \frac{\sum_{m \in \mathcal{D}_i} \|\Phi_{:, m}\| \|\Psi_{:, m}\|}{|\mathcal{D}_i|} \\ &\geq \exp\left(-\mathcal{O}((1+\sigma)(p_{\text{tail}}/p_{\min}) + \delta \cdot T)^2\right) \left(\frac{1}{1+\chi}\right)^2 p_{\min} \\ &\geq \frac{1 - \mathcal{O}\left((1+\sigma)(p_{\text{tail}}/p_{\min}) + \delta \cdot T\right)^2}{(1+\chi)^2} p_{\min} \end{aligned} \quad (\text{C50})$$

where we use  $\delta = \mathcal{O}(1/T)$ , Assumption 1, and the definition of  $p_{\min}$ .

Because

$$\frac{1 - \mathcal{O}\left((1+\sigma)(p_{\text{tail}}/p_{\min}) + \delta \cdot T\right)^2}{(1+\chi)^2} = \Omega\left(\frac{p_{\text{tail}}}{p_{\min}}\right), \quad (\text{C51})$$

we have

$$\inf_{1 \leq k \leq |\mathcal{D}_1|} s_k(G(\theta_1^*)) \geq \inf_{1 \leq k \leq |\mathcal{D}_1|} s_k(A(\theta_1^*)) - 2p_{\text{tail}} > \tau \geq 2p_{\text{tail}} \geq \sup_{k > |\mathcal{D}_1|} s_k(G(\theta_1^*)) \quad (\text{C52})$$

This guarantees that  $m_1 = |\mathcal{D}_{\pi_1}|$ .

**Step 4:** We show that  $m_i = 0$  when  $i > I$ .

For  $i > I$ , because of the block intervals from  $1 \leq i \leq I$ , we first have

$$\inf_j \text{dist}(\theta_i^*, I_j) \geq \frac{\alpha}{T} - \mathcal{O}\left((1+\sigma)\left(\frac{p_{\text{tail}}}{p_{\min}}\right)\frac{1}{T}\right) - \delta/2 \geq \frac{\alpha}{2T}, \quad (\text{C53})$$

where we use  $\alpha = \Omega(\chi^2 + (1+\sigma)^2(p_{\text{tail}}/p_{\min})^2)$  and  $\alpha = \mathcal{O}(\Delta \cdot T)$  in the last inequality. Using Theorem C.6 Eq. (C64), we have

$$\begin{aligned} G(\theta_i^*) &= \underbrace{\Phi_{:, \mathcal{D}} \cdot \text{diag}\left(\left\{\exp(-(\theta_i^* - \lambda_m)^2 T^2)\right\}_{m \in \mathcal{D}}\right) \cdot (\Psi_{:, \mathcal{D}})^\dagger}_{\|\cdot\|_2 \leq \sqrt{KLR} \exp(-\alpha^2/4)} \\ &\quad + \underbrace{\Phi_{:, \mathcal{D}^c} \cdot \text{diag}\left(\left\{\exp(-(\theta_i^* - \lambda_m)^2 T^2)\right\}_{m \in \mathcal{D}^c}\right) \cdot (\Psi_{:, \mathcal{D}^c})^\dagger + \mathcal{E}(\theta_i^*)}_{\|\cdot\|_2 \leq p_{\text{tail}}}. \end{aligned} \quad (\text{C54})$$

Because  $\alpha = \Omega(\log(KLR/p_{\text{tail}}))$ , we have

$$\|G(\theta_i^*)\|_2 \leq 2p_{\text{tail}} < \tau. \quad (\text{C55})$$

for  $i > I$ . This implies that  $m_i = 0$  for  $i > I$  and concludes the proof.  $\square$

### 1. Useful lemmas

**Lemma C.5.** Given  $\beta > 0$ . Let  $\{t_n\}$  to be i.i.d sampled from the truncated Gaussian  $a_T(t)$  defined as Eq. (16). Define

$$\mathcal{E}(\theta) := \frac{1}{N} \sum_{n=1}^N Z_n \exp(\mathbf{i}\theta t_n) - \Phi_{i,:} \cdot \text{diag}(\{\exp(-(\theta - \lambda_m)^2 T^2\}_{m \in [M]}) \cdot (\Psi^\dagger)_{:,j} \in \mathbb{C}^{L \times R}. \quad (\text{C56})$$

Let  $\Theta := \{\theta_j\}_{j=1}^J \cup \{\lambda_m\}_{m \in \mathcal{D}}$ .

If  $\sigma = \Omega\left(\log^{1/2}\left(\sqrt{LR}/\beta\right)\right)$  as in Eq. (16) and  $N = \Omega\left(\frac{LR}{\beta^2} \log\left((J + |\mathcal{D}|)\frac{LR}{\eta}\right)\right)$ , we have

$$\Pr\left[\max_{\theta \in \Theta} \|\mathcal{E}(\theta)\|_F \leq \beta\right] \geq 1 - \eta. \quad (\text{C57})$$

and

$$\Pr\left[\bigcap_{\theta, \theta' \in \Theta} \|\mathcal{E}(\theta) - \mathcal{E}(\theta')\|_F \leq \beta\sigma T|\theta - \theta'|\right] \geq 1 - \eta. \quad (\text{C58})$$

*Proof.* For each  $1 \leq i \leq L$  and  $1 \leq j \leq R$ , by Theorem C.7 with  $\tilde{\beta} = \frac{\beta}{\sqrt{LR}}$  and  $\tilde{\eta} = \frac{\eta}{LR}$ , we have

$$\Pr\left[\max_{\theta \in \Theta} |\mathcal{E}_{i,j}(\theta)| \leq \frac{\beta}{\sqrt{LR}}\right] \geq 1 - \frac{\eta}{LR}, \quad (\text{C59})$$

and

$$\Pr\left[\bigcap_{\theta, \theta' \in \Theta} \left\{ |\mathcal{E}_{i,j}(\theta) - \mathcal{E}_{i,j}(\theta')| \leq \frac{\beta}{\sqrt{LR}}\sigma T|\theta - \theta'|\right\}\right] \geq 1 - \frac{\eta}{LR}. \quad (\text{C60})$$

By union bound, the first equation implies that

$$\Pr\left[\max_{\theta \in \Theta} \|\mathcal{E}(\theta)\|_F = \max_{\theta \in \Theta} \sqrt{\sum_{i,j} |\mathcal{E}_{i,j}(\theta)|^2} \leq \beta\right] \geq \Pr\left[\bigcap_{i,j} \left\{ \max_{\theta \in \Theta} |\mathcal{E}_{i,j}(\theta)| \leq \frac{\beta}{\sqrt{LR}}\right\}\right] \geq 1 - \eta. \quad (\text{C61})$$

And the second equation implies

$$\begin{aligned} & \Pr\left[\bigcap_{\theta, \theta' \in \Theta} \|\mathcal{E}(\theta) - \mathcal{E}(\theta')\|_F = \sqrt{\sum_{i,j} |\mathcal{E}_{i,j}(\theta) - \mathcal{E}_{i,j}(\theta')|^2} \leq \beta\sigma T|\theta - \theta'|\right] \\ & \geq \Pr\left[\bigcap_{i,j} \left\{ \bigcap_{\theta, \theta' \in \Theta} |\mathcal{E}_{i,j}(\theta) - \mathcal{E}_{i,j}(\theta')| \leq \frac{\beta}{\sqrt{LR}}\sigma T|\theta - \theta'|\right\}\right] \geq 1 - \eta. \end{aligned} \quad (\text{C62})$$

This completes the proof of the lemma.  $\square$

**Lemma C.6.** Given any matrix  $\Phi \in \mathbb{C}^{L \times M}, \Psi \in \mathbb{C}^{R \times M}$ , and  $\{\lambda_m\}_{m \in [M]}$ . Define

$$G(\theta) = \Phi \cdot \text{diag}(\{\exp(-(\theta - \lambda_m)^2 T^2)\}_{m \in [M]}) \cdot \Psi^\dagger. \quad (\text{C63})$$

We have

$$\|G(\theta)\|_F \leq \left(\max_m \exp(-(\theta - \lambda_m)^2 T^2)\right) \sum_{m \in [M]} \sqrt{\left(\sum_{l=1}^L |\Phi_{l,m}|^2\right) \left(\sum_{r=1}^R |\Psi_{r,m}|^2\right)} \quad (\text{C64})$$

and

$$\begin{aligned} \|G(\theta) - G(\theta')\|_F &\leq T|\theta - \theta'| \sum_{m \in [M]} \|\Phi_{:,m} \Psi_{:,m}^\dagger\|_F \\ &\leq T|\theta - \theta'| \sum_{m \in [M]} \sqrt{\left(\sum_{l=1}^L |\Phi_{l,m}|^2\right) \left(\sum_{r=1}^R |\Psi_{r,m}|^2\right)} \end{aligned} \quad (\text{C65})$$

*Proof.* First, we note that

$$\begin{aligned} \|G(\theta)\|_F &\leq \sum_{m \in [M]} \|\Phi_{:,m} \exp(-(\theta - \lambda_m)^2 T^2) \Psi_{:,m}^\dagger\|_F \\ &\leq \left(\max_m \exp(-(\theta - \lambda_m)^2 T^2)\right) \sum_{m \in [M]} \|\Phi_{:,m} \Psi_{:,m}^\dagger\|_F \\ &= \left(\max_m \exp(-(\theta - \lambda_m)^2 T^2)\right) \sum_{m \in [M]} \sqrt{\left(\sum_{l=1}^L |\Phi_{l,m}|^2\right) \left(\sum_{r=1}^R |\Psi_{r,m}|^2\right)} \end{aligned} \quad (\text{C66})$$

This concludes the proof of Eq. (C64).

Second, we have

$$\begin{aligned} &\|G(\theta) - G(\theta')\|_F \\ &\leq \sum_{m \in [M]} \|\Phi_{:,m} (\exp(-(\theta - \lambda_m)^2 T^2) - \exp(-(\theta' - \lambda_m)^2 T^2)) \Psi_{:,m}^\dagger\|_F \\ &\leq \left(\max_m (\exp(-(\theta - \lambda_m)^2 T^2) - \exp(-(\theta' - \lambda_m)^2 T^2))\right) \sum_{m \in [M]} \|\Phi_{:,m} \Psi_{:,m}^\dagger\|_F \\ &\leq T|\theta - \theta'| \sum_{m \in [M]} \|\Phi_{:,m} \Psi_{:,m}^\dagger\|_F \\ &= T|\theta - \theta'| \sum_{m \in [M]} \sqrt{\left(\sum_{l=1}^L |\Phi_{l,m}|^2\right) \left(\sum_{r=1}^R |\Psi_{r,m}|^2\right)}, \end{aligned} \quad (\text{C67})$$

where the last step follows from the 1-Lipschitzness of  $\exp(-x^2)$ .

This concludes the proof of Eq. (C65).  $\square$

**Lemma C.7** ([23, Lemma A.1]). *Given  $\tilde{\beta} > 0$ ,  $i \in [L]$ ,  $j \in [R]$ . Let  $\{t_n\}$  to be i.i.d sampled from the truncated Gaussian  $a_T^{\text{trunc}}(t)$  defined as Eq. (16). Define*

$$\mathcal{E}_{i,j}(\theta) := \frac{1}{N} \sum_{n=1}^N (Z_n)_{i,j} \exp(\mathbf{i}\theta t_n) - \Phi_{i,:} \cdot \text{diag}(\{\exp(-(\theta - \lambda_m)^2 T^2)\}_{m \in [M]}) \cdot (\Psi^\dagger)_{:,j} \in \mathbb{C}. \quad (\text{C68})$$

Let  $\Theta := \{\theta_j\}_{j=1}^J \cup \{\lambda_m\}_{m \in \mathcal{D}}$ . If  $\sigma = \Omega\left(\log^{1/2}(1/\tilde{\beta})\right)$  and  $N = \Omega\left(\frac{1}{\tilde{\beta}^2} \log\left((J + |\mathcal{D}|)\frac{1}{\tilde{\eta}}\right)\right)$ , we have

$$\Pr\left[\max_{\theta \in \Theta} |\mathcal{E}_{i,j}(\theta)| > \tilde{\beta}\right] \leq 1 - \tilde{\eta}, \quad (\text{C69})$$

and<sup>iii</sup>

$$\Pr\left[\bigcap_{\theta, \theta' \in \Theta} |\mathcal{E}_{i,j}(\theta) - \mathcal{E}_{i,j}(\theta')| \leq \tilde{\beta}\sigma T|\theta - \theta'|\right] \geq 1 - \tilde{\eta}. \quad (\text{C70})$$

<sup>iii</sup> In fact, [23, Lemma A.1] has extra  $\beta^2$  on the RHS of the inequality inside the probability in the equation below, which is unnecessary.

## Appendix D: Analysis of the observable estimation

In this section, we give the proof of [Theorem V.1](#). In addition to the assumption in [Theorem C.2](#), we assume  $\delta = 0$ ,  $p_{\text{tail}} = 0$ ,  $p_{\min} = \Omega(1)$ , and  $K, L, R = \mathcal{O}(1)$ . Following the proof of [Theorem C.2](#), when  $T = \tilde{\Omega}(\Delta^{-1})$  and  $N = \Omega(1)$ , we first have

$$\sup_{1 \leq j \leq I} |\theta_j^* - \lambda_{\pi(j)}^*| \leq \Delta/4. \quad (\text{D1})$$

This implies  $\theta_j^*$  is at least  $\Delta/2$  away from  $\lambda_i^*$  when  $i \neq \pi(j)$ .

Now, we improve the above bound and aim to show

$$\sup_{1 \leq j \leq I} |\theta_j^* - \lambda_{\pi(j)}^*| = \mathcal{O}\left(\frac{1}{T} \left(\exp(-\Delta^2 T^2/32) + N^{-1/2}\right)\right). \quad (\text{D2})$$

Without loss of generality, we consider  $j = 1$ . Because  $p_{\text{tail}} = 0$ , we have

$$\begin{aligned} G(\theta) &= \underbrace{\Phi_{:, \mathcal{D}_{\pi_1}} \cdot \text{diag}\left(\{\exp(-(\theta - \lambda_m)^2 T^2)\}_{m \in \mathcal{D}_{\pi_1}}\right) \cdot (\Psi_{:, \mathcal{D}_{\pi_1}})^\dagger}_{:= A(\theta)} \\ &+ \underbrace{\Phi_{:, \mathcal{D}^c} \cdot \text{diag}\left(\{\exp(-(\theta - \lambda_m)^2 T^2)\}_{m \in \mathcal{D}^c}\right) \cdot (\Psi_{:, \mathcal{D}^c})^\dagger}_{= 0} \\ &+ \underbrace{\sum_{i \neq \pi_1} \Phi_{:, \mathcal{D}_i} \cdot \text{diag}\left(\{\exp(-(\theta - \lambda_m)^2 T^2)\}_{m \in \mathcal{D}_i}\right) \cdot (\Psi_{:, \mathcal{D}_i})^\dagger + \mathcal{E}(\theta)}_{:= C(\theta)}. \end{aligned} \quad (\text{D3})$$

Because  $K, L, R = \mathcal{O}(1)$  and  $|\theta_1^* - \lambda_j^*| \geq \Delta/2$  for  $j \neq \pi_1$ , we first have  $|\theta_1^* - \lambda_m| \geq \Delta/4$  if the dominant index  $m \notin \mathcal{D}_{\pi_1}$ . This implies

$$\|C(\theta)\|_F = \mathcal{O}(\exp(-\Delta^2 T^2/16)), \quad (\text{D4})$$

and

$$\|G(\theta) - A(\theta) - \mathcal{E}(\theta)\|_F = \mathcal{O}(\exp(-\Delta^2 T^2/16)). \quad (\text{D5})$$

Using [Theorem C.7](#), with high probability, we also have

$$\mathcal{E}(\theta) = \tilde{\mathcal{O}}(N^{-1/2}), \quad \|\mathcal{E}(\theta) - \mathcal{E}(\theta')\|_F = \mathcal{O}(\sigma T |\theta - \theta'| N^{-1/2}). \quad (\text{D6})$$

Let  $\tilde{\theta}_1^*$  be the closest energy grid point to the desired cluster center  $\lambda_{\pi_1}^*$ . Similar to [Eq. \(C44\)](#) in the second step of the proof of [Theorem C.2](#), we have

$$\begin{aligned} &2\text{Re}(\text{Tr}(A^\dagger(\theta_1^*) \mathcal{E}(\theta_1^*))) - 2\text{Re}(\text{Tr}(A^\dagger(\tilde{\theta}_1^*) \mathcal{E}(\tilde{\theta}_1^*))) \\ &= \mathcal{O}\left(T |\theta_1^* - \tilde{\theta}_1^*| N^{-1/2} + \sigma T |\theta_1^* - \tilde{\theta}_1^*| N^{-1/2}\right) \\ &= \mathcal{O}\left((1 + \sigma)T \left(|\theta_1^* - \lambda_{\pi_1}^*| + \frac{q}{T}\right) N^{-1/2}\right) \end{aligned} \quad (\text{D7})$$

Choosing  $q = \tilde{\mathcal{O}}(N^{-1/2})$ , similar to [Eq. \(C45\)](#), we have

$$\begin{aligned} &\underbrace{\left(\exp\left(-2(\tilde{\theta}_1^* - \lambda_{\pi_1}^*)^2 T^2\right) - \exp\left(-2(\theta_1^* - \lambda_{\pi_1}^*)^2 T^2\right)\right)}_{\leq 0} \\ &= \mathcal{O}\left(T |\theta_1^* - \lambda_{\pi_1}^*| N^{-1/2} + \frac{1}{N} + \exp(-\Delta^2 T^2/16)\right). \end{aligned} \quad (\text{D8})$$

Following a similar calculation as [Eq. \(C46\)](#), we have

$$T |\theta_1^* - \lambda_{\pi_1}^*| = \mathcal{O} \left( \frac{1}{\sqrt{N}} + \exp(-\Delta^2 T^2 / 32) \right). \quad (\text{D9})$$

We conclude proof of [Eq. \(D2\)](#).

Next, we consider the observation data matrix error. For a fixed  $i$ , we define the exact data matrix for the generalized eigenvalue problem:

$$G_{\text{exact}} = \Phi_{:, [m_i]} (\Psi_{:, [m_i]})^\dagger, \quad G_{\text{exact}}^O = \Phi_{:, [m_i]} \cdot O_{\mathcal{D}_i} \cdot (\Psi_{:, [m_i]})^\dagger, \quad (\text{D10})$$

where  $O_{\mathcal{D}_i}$  is defined in [Eq. \(37\)](#). According to [Eq. \(D2\)](#), [Theorem C.5](#), and following a similar calculation as [Eq. \(53\)](#), we have

$$\begin{aligned} \|G(\theta_i^*) - G_{\text{exact}}\|_2 &= \mathcal{O} \left( \frac{1}{\sqrt{N}} + \exp(-\Delta^2 T^2 / 16) \right), \\ \|G^O(\theta_i^*) - G_{\text{exact}}^O\|_2 &= \mathcal{O} \left( \|O\| \left( \frac{1}{\sqrt{N}} + \exp(-\Delta^2 T^2 / 16) \right) \right), \end{aligned} \quad (\text{D11})$$

where  $G(\theta_i^*)$  and  $G^O(\theta_i^*)$  are defined in [Eqs. \(18\)](#) and [\(32\)](#), respectively.

According to [Assumption 1](#),  $G_{\text{exact}}$  has rank  $m_i$  with smallest nonzero singular value lower bounded by  $p_{\min}/(1+\chi)$ . Combining this and [Eq. \(D11\)](#),  $|m_i|$ -th singular value of  $G(\theta_i^*)$  can be lower bound by  $p_{\min}/(2(1+\chi))$  when  $T = \Omega(\Delta^{-1})$  and  $N = \Omega(1)$ . Furthermore, following the third step of the proof of [Theorem C.2](#), the  $(m_i + 1)$ -th singular value of  $G(\theta_i^*)$  can be upper bound by  $p_{\min}/(4(1 + \chi))$  when  $T = \Omega(\Delta^{-1})$  and  $N = \Omega(1)$ . Using singular value perturbation theory, these imply that

$$\begin{aligned} \|\tilde{G}(\theta_i^*) - \tilde{G}_{\text{exact}}\|_2 &= \mathcal{O} \left( \frac{1}{\sqrt{N}} + \exp(-\Delta^2 T^2 / 32) \right), \\ \|\tilde{G}^O(\theta_i^*) - \tilde{G}_{\text{exact}}^O\|_2 &= \mathcal{O} \left( \|O\| \left( \frac{1}{\sqrt{N}} + \exp(-\Delta^2 T^2 / 32) \right) \right), \end{aligned} \quad (\text{D12})$$

where  $\tilde{G}_{\text{exact}}$  and  $\tilde{G}_{\text{exact}}^O$  are defined using the same forms as [Eq. \(34\)](#). Here, both  $\tilde{G}(\theta_i^*)$  and  $\tilde{G}_{\text{exact}}$  are full rank matrices with smallest singular value lower bounded by  $p_{\min}/(2(1 + \chi))$ . According to generalized eigenvalue perturbation theory, we finally have

$$|\lambda_k^O - \lambda_{k, \text{exact}}| = \mathcal{O} \left( \|O\| \left( \frac{1}{\sqrt{N}} + \exp(-\Delta^2 T^2 / 32) \right) \right), \quad (\text{D13})$$

where  $\lambda_{k, \text{exact}}$  is the  $k$ -th generalized eigenvalue:  $\tilde{G}_{\text{exact}}^O = \lambda_k \tilde{G}_{\text{exact}}$ .

Therefore to achieve  $\epsilon_O$  precision in  $\lambda_k^O$ , it is required that  $N = \tilde{\Omega}(\epsilon_O^{-2})$  and  $T = \tilde{\mathcal{O}}(\Delta^{-1})$ . This concludes the proof.

---

[1] X.-G. Wen, Colloquium: Zoo of quantum-topological phases of matter, [Rev. Mod. Phys. 89, 041004 \(2017\)](#).

[2] C. Nayak, S. H. Simon, A. Stern, M. Freedman, and S. Das Sarma, Non-abelian anyons and topological quantum computation, [Rev. Mod. Phys. 80, 1083 \(2008\)](#).

[3] B. Brown, S. T. Flammia, and N. Schuch, Computational difficulty of computing the density of states, [Phys. Rev. Lett. 107, 040501 \(2011\)](#).

[4] F. G. S. L. Brandao, Entanglement theory and the quantum simulation of many-body physics (2008), [arXiv:0810.0026 \[quant-ph\]](#).

[5] C. Gyurik, C. Cade, and V. Dunjko, Towards quantum advantage via topological data analysis, [Quantum 6, 855 \(2022\)](#).

[6] Y. Yang, A. Christianen, M. C. Bañuls, D. S. Wild, and J. I. Cirac, Phase-sensitive quantum measurement without controlled operations, [Phys. Rev. Lett. 132, 220601 \(2024\)](#).

[7] L. Clinton, T. S. Cubitt, R. Garcia-Patron, A. Montanaro, S. Stanisic, and M. Stroeks, Quantum phase estimation without controlled unitaries (2024), [arXiv:2410.21517 \[quant-ph\]](#).

[8] X. Wang, L. Xiong, X. Cai, and X. Yuan, Computing  $n$ -time correlation functions without ancilla qubits (2025), [arXiv:2504.12975 \[quant-ph\]](#).

[9] B. F. Schiffer, D. S. Wild, N. Maskara, M. D. Lukin, and J. I. Cirac, Hardware-efficient quantum phase estimation via local control (2025), [arXiv:2506.18765 \[quant-ph\]](#).

[10] C. Yi and C. Zhou, Ancilla-free quantum protocol for thermal Green's functions (2025), [arXiv:2509.03288 \[quant-ph\]](https://arxiv.org/abs/2509.03288).

[11] P. Zeng, J. Sun, and X. Yuan, Universal quantum algorithmic cooling on a quantum computer (2022), [arXiv:2109.15304 \[quant-ph\]](https://arxiv.org/abs/2109.15304).

[12] R. Zhang, G. Wang, and P. Johnson, Computing ground state properties with early fault-tolerant quantum computers, *Quantum* **6**, 761 (2022).

[13] J. Sun, P. Zeng, T. Gur, and M. S. Kim, High-precision and low-depth eigenstate property estimation: theory and resource estimation (2024), [arXiv:2406.04307 \[quant-ph\]](https://arxiv.org/abs/2406.04307).

[14] J. Sun and P. Zeng, Randomised composite linear-combination-of-unitaries: its role in quantum simulation and observable estimation (2025), [arXiv:2506.15658 \[quant-ph\]](https://arxiv.org/abs/2506.15658).

[15] A. Y. Kitaev, Quantum measurements and the abelian stabilizer problem (1995), [arXiv:quant-ph/9511026 \[quant-ph\]](https://arxiv.org/abs/quant-ph/9511026).

[16] A. Y. Kitaev, A. H. Shen, and M. N. Vyalyi, *Classical and Quantum Computation* (American Mathematical Society, USA, 2002).

[17] M. Dobšíček, G. Johansson, V. Shumeiko, and G. Wendin, Arbitrary accuracy iterative quantum phase estimation algorithm using a single ancillary qubit: A two-qubit benchmark, *Phys. Rev. A* **76**, 030306 (2007).

[18] N. Wiebe and C. Granade, Efficient Bayesian phase estimation, *Phys. Rev. Lett.* **117**, 010503 (2016).

[19] R. D. Somma, Quantum eigenvalue estimation via time series analysis, *New J. Phys.* **21**, 123025 (2019).

[20] T. E. O'Brien, B. Tarasinski, and B. M. Terhal, Quantum phase estimation of multiple eigenvalues for small-scale (noisy) experiments, *New J. Phys.* **21**, 023022 (2019).

[21] Z. Ding and L. Lin, Even shorter quantum circuit for phase estimation on early fault-tolerant quantum computers with applications to ground-state energy estimation, *PRX Quantum* **4**, 020331 (2023).

[22] Z. Ding and L. Lin, Simultaneous estimation of multiple eigenvalues with short-depth quantum circuit on early fault-tolerant quantum computers, *Quantum* **7**, 1136 (2023).

[23] Z. Ding, H. Li, L. Lin, H. Ni, L. Ying, and R. Zhang, Quantum multiple eigenvalue gaussian filtered search: an efficient and versatile quantum phase estimation method, *Quantum* **8**, 1487 (2024).

[24] Z. Ding, Y. Dong, Y. Tong, and L. Lin, Robust ground-state energy estimation under depolarizing noise (2024), [arXiv:2307.11257 \[quant-ph\]](https://arxiv.org/abs/2307.11257).

[25] C. Yi, C. Zhou, and J. Takahashi, Quantum phase estimation by compressed sensing, *Quantum* **8**, 1579 (2024).

[26] D. Castaldo and S. Corni, Heisenberg limited multiple eigenvalue estimation via off-the-grid compressed sensing (2025), [arXiv:2507.12438 \[quant-ph\]](https://arxiv.org/abs/2507.12438).

[27] H. Ni, H. Li, and L. Ying, On low-depth algorithms for quantum phase estimation, *Quantum* **7**, 1165 (2023).

[28] G. Wang, D. S. França, R. Zhang, S. Zhu, and P. D. Johnson, Quantum algorithm for ground state energy estimation using circuit depth with exponentially improved dependence on precision, *Quantum* **7**, 1167 (2023).

[29] H. Li, H. Ni, and L. Ying, Adaptive low-depth quantum algorithms for robust multiple-phase estimation, *Phys. Rev. A* **108**, 062408 (2023).

[30] R. M. Parrish and P. L. McMahon, Quantum filter diagonalization: Quantum eigendecomposition without full quantum phase estimation, preprint [10.48550/arXiv.1909.08925](https://arxiv.org/abs/1909.08925) (2019).

[31] W. J. Huggins, J. Lee, U. Baek, B. O'Gorman, and K. B. Whaley, A non-orthogonal variational quantum eigensolver, *New J. Phys.* **22**, 073009 (2020).

[32] N. H. Stair, R. Huang, and F. A. Evangelista, A multireference quantum Krylov algorithm for strongly correlated electrons, *J. Chem. Theory Comput.* **16**, 2236 (2020).

[33] K. Seki and S. Yunoki, Quantum power method by a superposition of time-evolved states, *PRX Quantum* **2**, 1 (2021).

[34] E. N. Epperly, L. Lin, and Y. Nakatsukasa, a theory of quantum subspace diagonalization, *SIMAX* **43**, 1263 (2022).

[35] U. Baek, D. Hait, J. Shee, O. Leimkuhler, W. J. Huggins, T. F. Stetina, M. Head-Gordon, and K. B. Whaley, Say NO to optimization: A non-orthogonal quantum eigensolver, *PRX Quantum* **4**, 1 (2022).

[36] W. Kirby, Analysis of quantum Krylov algorithms with errors, *Quantum* **8**, 1 (2024).

[37] N. Yoshioka, M. Amico, W. Kirby, P. Jurcevic, A. Dutt, B. Fuller, S. Garion, H. Haas, I. Hamamura, A. Ivrii, R. Majumdar, Z. Minev, M. Motta, B. Pokharel, P. Rivero, K. Sharma, C. J. Wood, A. Javadi-Abhari, and A. Mezzacapo, Krylov diagonalization of large many-body Hamiltonians on a quantum processor, *Nat. Commun.* **16**, 1 (2025).

[38] A. Peruzzo, J. McClean, P. Shadbolt, M.-H. Yung, X.-Q. Zhou, P. J. Love, A. Aspuru-Guzik, and J. L. O'Brien, A variational eigenvalue solver on a photonic quantum processor, *Nat. Commun.* **5**, 4213 (2014).

[39] E. Farhi, J. Goldstone, and S. Gutmann, A quantum approximate optimization algorithm (2014), [arXiv:1411.4028 \[quant-ph\]](https://arxiv.org/abs/1411.4028).

[40] A. Kandala, A. Mezzacapo, K. Temme, M. Takita, M. Brink, J. M. Chow, and J. M. Gambetta, Hardware-efficient variational quantum eigensolver for small molecules and quantum magnets, *Nature* **549**, 242 (2017).

[41] M. Motta, C. Sun, A. T. Tan, M. J. O'Rourke, E. Ye, A. J. Minnich, F. G. Brandão, and G. K. L. Chan, Determining eigenstates and thermal states on a quantum computer using quantum imaginary time evolution, *Nat. Phys.* **16**, 205 (2020).

[42] S.-H. Lin, R. Dilip, A. G. Green, A. Smith, and F. Pollmann, Real- and imaginary-time evolution with compressed quantum circuits, *PRX Quantum* **2**, 010342 (2021).

[43] X. Yuan, S. Endo, Q. Zhao, Y. Li, and S. C. Benjamin, Theory of variational quantum simulation, *Quantum* **3**, 1 (2019).

[44] D. Slepian, Prolate spheroidal wave functions, fourier analysis, and uncertainty — v: the discrete case, *BSTJ* **57**, 1371 (1978).

[45] J. Kaiser and R. Schafer, On the use of the i0-sinh window for spectrum analysis, *IEEE Trans. Acoust. Speech Signal Process.* **28**, 105 (1980).

[46] D. B. Percival and A. T. Walden, *Spectral Analysis for Physical Applications* (Cambridge University Press, 1993).

[47] Y. Dong, L. Lin, and Y. Tong, Ground-state preparation and energy estimation on early fault-tolerant quantum computers via quantum eigenvalue transformation of unitary matrices, *PRX Quantum* **3**, 040305 (2022).

[48] T. Kosugi, Y. Nishiya, H. Nishi, and Y.-i. Matsushita, Imaginary-time evolution using forward and backward real-time evolution with a single ancilla: First-quantized eigensolver algorithm for quantum chemistry, *Phys. Rev. Res.* **4**, 033121 (2022).

[49] G. Vidal, Efficient simulation of one-dimensional quantum many-body systems, *Phys. Rev. Lett.* **93**, 040502 (2004).

[50] A. Kitaev, Fault-tolerant quantum computation by anyons, *Annals of Physics* **303**, 2 (2003).

[51] K. J. Satzinger, Y. J. Liu, A. Smith, C. Knapp, M. Newman, C. Jones, Z. Chen, C. Quintana, X. Mi, A. Dunsworth, C. Gidney, I. Aleiner, F. Arute, K. Arya, J. Atalaya, R. Babbush, J. C. Bardin, R. Barends, J. Basso, A. Bengtsson, A. Bilmes, M. Broughton, B. B. Buckley, D. A. Buell, B. Burkett, N. Bushnell, B. Chiaro, R. Collins, W. Courtney, S. Demura, A. R. Derk, D. Eppens, C. Erickson, L. Faoro, E. Farhi, A. G. Fowler, B. Foxen, M. Giustina, A. Greene, J. A. Gross, M. P. Harrigan, S. D. Harrington, J. Hilton, S. Hong, T. Huang, W. J. Huggins, L. B. Ioffe, S. V. Isakov, E. Jeffrey, Z. Jiang, D. Kafri, K. Kechedzhi, T. Khattar, S. Kim, P. V. Klimov, A. N. Korotkov, F. Kostritsa, D. Landhuis, P. Laptev, A. Locharla, E. Lucero, O. Martin, J. R. McClean, M. McEwen, K. C. Miao, M. Mohseni, S. Montazeri, W. Mruczkiewicz, J. Mutus, O. Naaman, M. Neeley, C. Neill, M. Y. Niu, T. E. O'Brien, A. Opremcak, B. Pató, A. Petukhov, N. C. Rubin, D. Sank, V. Shvarts, D. Strain, M. Szalay, B. Villalonga, T. C. White, Z. Yao, P. Yeh, J. Yoo, A. Zalcman, H. Neven, S. Boixo, A. Megrant, Y. Chen, J. Kelly, V. Smelyanskiy, A. Kitaev, M. Knap, F. Pollmann, and P. Roushan, Realizing topologically ordered states on a quantum processor, *Science* **374**, 1237 (2021).

[52] T. G. Kolda and B. W. Bader, Tensor decompositions and applications, *SIAM Review* **51**, 455 (2009).

[53] R. A. Harshman *et al.*, Foundations of the parafac procedure: Models and conditions for an “explanatory” multi-modal factor analysis, *UCLA working papers in phonetics* **16**, 84 (1970).

[54] J. D. Carroll and J. J. Chang, Analysis of individual differences in multidimensional scaling via an n-way generalization of “Eckart-Young” decomposition, *Psychometrika* **35**, 283 (1970).

[55] S. E. Leurgans, R. T. Ross, and R. B. Abel, A decomposition for three-way arrays, *SIAM J. Matrix Anal. Appl.* **14**, 1064–1083 (1993).

[56] R. Bro, Parafac. tutorial and applications, *Chemometr Intell Lab Syst* **38**, 149 (1997).

[57] V. Sharan and G. Valiant, Orthogonalized als: A theoretically principled tensor decomposition algorithm for practical use, in *ICML* (PMLR, 2017) pp. 3095–3104.

[58] F. Roemer, M. Haardt, and G. Del Galdo, Analytical performance assessment of multi-dimensional matrix- and tensor-based esprit-type algorithms, *IEEE Trans. Signal Process.* **62**, 2611 (2014).

[59] D. Hangleiter, I. Roth, J. Fuksa, J. Eisert, and P. Roushan, Robustly learning the Hamiltonian dynamics of a superconducting quantum processor, *Nat. Commun.* **15**, 1 (2024).

[60] H. L. Stormer, D. C. Tsui, and A. C. Gossard, The fractional quantum hall effect, *Rev. Mod. Phys.* **71**, S298 (1999).

[61] N. Regnault and B. A. Bernevig, Fractional chern insulator, *Phys. Rev. X* **1**, 021014 (2011).

[62] A. Pal and D. A. Huse, Many-body localization phase transition, *Phys. Rev. B* **82**, 174411 (2010).

[63] D. A. Abanin, E. Altman, I. Bloch, and M. Serbyn, Colloquium: Many-body localization, thermalization, and entanglement, *Rev. Mod. Phys.* **91**, 021001 (2019).

[64] C. J. Turner, A. A. Michailidis, D. A. Abanin, M. Serbyn, and Z. Papić, Weak ergodicity breaking from quantum many-body scars, *Nat. Phys.* **14**, 745 (2018).

[65] C. J. Lin and O. I. Motrunich, Exact quantum many-body scar states in the rydberg-blockaded atom chain, *Phys. Rev. Lett.* **122**, 173401 (2019).

[66] A. Chandran, T. Iadecola, V. Khemani, and R. Moessner, Quantum many-body scars: A quasiparticle perspective, *Annu. Rev. Condens. Matter Phys.* **14**, 443 (2023).

[67] Z. Ding, E. N. Epperly, L. Lin, and R. Zhang, The ESPRIT algorithm under high noise: Optimal error scaling and noisy super-resolution, in *FOCS* (2024) pp. 2344–2366.